**SANDIA REPORT**
SAND2013-1863
Unlimited Release
Printed March 12, 2013

# Penetration of rod projectiles in semi-infinite targets: a validation test for Eulerian X-FEM in ALEGRA

Byoung Yoon Park[1], R. Brian Leavy[2], and John H. J. Niederhaus[1]

[1] Sandia National Laboratories
[2] U.S. Army Research Laboratory

Prepared by
Sandia National Laboratories
Albuquerque, New Mexico 87185 and Livermore, California 94550

Sandia National Laboratories is a multi-program laboratory managed and operated by Sandia Corporation, a wholly owned subsidiary of Lockheed Martin Corporation, for the U.S. Department of Energy's National Nuclear Security Administration under contract DE-AC04-94AL85000.



Issued by Sandia National Laboratories, operated for the United States Department of Energy by Sandia Corporation.



Available to DOE and DOE contractors from
U.S. Department of Energy
Office of Scientific and Technical Information
P.O. Box 62
Oak Ridge, TN 37831

Telephone: (865) 576-8401
Facsimile: (865) 576-5728
E-Mail: reports@adonis.osti.gov
Online ordering: http://www.osti.gov/bridge

Available to the public from
U.S. Department of Commerce
National Technical Information Service
5285 Port Royal Rd.
Springfield, VA 22161

Telephone: (800) 553-6847
Facsimile: (703) 605-6900
E-Mail: orders@ntis.fedworld.gov
Online order: http://www.ntis.gov/help/ordermethods.asp?loc=7-4-0#online

SAND2013-1863
Unlimited Release
Printed March 2013

# Penetration of rod projectiles in semi-infinite targets: a validation test for Eulerian X-FEM in ALEGRA

Byoung Yoon Park[1], R. Brian Leavy[2], and John H. J. Niederhaus[3]

[1]-Geomechanics Department
Sandia National Laboratories
P.O. Box 5800
Albuquerque, NM 87185-MS0751

[2]-Impact Physics Branch
U.S. Army Research Laboratory
ATTN: RDRL-WMP-C
Aberdeen Proving Grounds, MD 21005

[3]- Computational Shock and Multiphysics
Sandia National Laboratories
P.O. Box 5800
Albuquerque, NM 87185-MS1323

## Abstract

The finite-element shock hydrodynamics code ALEGRA has recently been upgraded to include an X-FEM implementation in 2D for simulating impact, sliding, and release between materials in the Eulerian frame. For validation testing purposes, the problem of long-rod penetration in semi-infinite targets is considered in this report, at velocities of 500 to 3000 m/s. We describe testing simulations done using ALEGRA with and without the X-FEM capability, in order to verify its adequacy by showing X-FEM recovers the good results found with the standard ALEGRA formulation. The X-FEM results for depth of penetration differ from previously measured experimental data by less than 2%, and from the standard formulation results by less than 1%. They converge monotonically under mesh refinement at first order. Sensitivities to domain size and rear boundary condition are investigated and shown to be small. Aside from some simulation stability issues, X-FEM is found to produce good results for this classical impact and penetration problem.

# ACKNOWLEDGMENTS

The authors would like to acknowledge the valuable contributions to this work provided by the U.S. Army Research Laboratory (ARL). Thanks to Andy Porwitzky (ARL) who provided helpful technical comments on the results. Thanks to Bill Rider (Org. 1443), who provided useful assistance with convergence analysis for the computational penetration results. We also would like to thank the Sandia managers who oversaw the project, Erik Strack and Tom Pfeifle. Finally, we would like to thank the ALEGRA development team (Org. 1443), particularly the XFEM developers Tom Voth and Stewart Mosso.

# CONTENTS

ACKNOWLEDGMENTS ..... 4
CONTENTS ..... 5
FIGURES ..... 6
TABLES ..... 7
NOMENCLATURE ..... 8
1. INTRODUCTION ..... 9
1.1. Background ..... 9
1.2. Numerical methods ..... 9
2. EXPERIMENTAL DATA ..... 11
3. MODEL DESCRIPTION ..... 13
4. ANALYSIS RESULTS ..... 16
4.1. Depth of penetration ..... 16
4.2. Mesh resolution ..... 18
4.3. Comparison to the standard finite-element algorithms ..... 25
4.4. Model boundary condition and geometry effect ..... 29
4.4.1. Target boundary ..... 30
4.4.2. Target plate thickness ..... 32
4.4.3. Target plate radius ..... 34
5. SUMMARY AND CONCLUSIONS ..... 36
6. REFERENCES ..... 38
APPENDIX: INPUT DECK ..... 40
Appendix 1: Input deck for 4x12fixed ..... 40
Appendix 2: Input deck for 4x18fixed ..... 51
Appendix 3: Input deck for 5x12fixed ..... 55
DISTRIBUTION ..... 59

# FIGURES

Figure 1: Heaviside enrichment in X-FEM. Nodes are indexed by *J*, and materials by *m*, within a single element in the computational mesh. Interface intersections are green. ..... 10
Figure 2: Experimental data from a penetration mechanics database [2]: the penetration depth *P* normalized by the projectile length *L* as a function of the projectile velocity $V_P$, with empirical data fits based on the Lanz-Odermatt formula [12] and a 5th-order polynomial. 12
Figure 3: Schematic diagram and boundary conditions of the model with denotation of each parameter. ..... 14
Figure 4: Calculation of DOP for the baseline case with V_ROD=3000 m/s. ..... 17
Figure 5: Simulation results at 0 and 49 μs for the baseline case with V_ROD=3000 m/s (Unit on axes is m). ..... 17
Figure 6: Computational mesh for uniform cell size=0.5 mm (Unit on axes: m). ..... 19
Figure 7: Computational mesh for uniform cell size=0.25 mm (Unit on axes: m). ..... 19
Figure 8: Computational mesh for uniform cell size=0.125 mm (Unit on axes: m). ..... 20
Figure 9: Computational mesh for graded cell size=0.2 mm (Unit on axes: m). ..... 20
Figure 10: Computational mesh for graded cell size=0.15 mm (Unit on axes: m). ..... 21
Figure 11: Computational mesh for graded cell size=0.1 mm (Unit on axes: m). ..... 21
Figure 12: Predicted DOP, rod head and plate surface histories with VP=1500 m/s from X-FEM simulation using the mesh with various cell sizes. ..... 22
Figure 13: Depths of penetration with $V_P$=1500 m/s from X-FEM simulation using the mesh with various cell sizes. ..... 23
Figure 14: Mesh sensitivity for X-FEM and standard ALEGRA ("U-FEM") results. ..... 24
Figure 15: Predicted DOP, rod head and plate surface histories from X-FEM with six velocities of rod. ..... 25
Figure 16: Comparison between the experimental data with predicted normalized penetration depths from X-FEM simulation. ..... 26
Figure 17: Comparison between the predicted normalized penetration depths from X-FEM, *aggressive* and *donor* aggressive simulations, and experimental data. ..... 26
Figure 18: Simulation results using X-FEM algorithm with projectile velocity 3000 m/s. Contours of the axial velocity are plotted on the left, and contours of the material number on the right. Simulation times are 12, 30, 50 and 100 μs. ..... 28
Figure 19: Computational mesh used to examine target plate thickness (Unit on axes: m). ..... 29
Figure 20: Computational mesh used to examine the target plate radius. (Unit on axes: m). ..... 30
Figure 21: Comparison of the normalized penetration depths from the models with plate back fixed (Baseline) and plate back free boundary conditions. ..... 31
Figure 22: Predicted DOP, rod head and plate surface histories with six velocities of rod from the model with plate back free boundary condition. ..... 32
Figure 23: Comparison of the normalized penetration depths from the models with plate thicknesses of 12 cm (Baseline) and 18 cm. ..... 33
Figure 24: Predicted DOP, rod head and plate surface histories with six velocities of rod from the model with target plate thickness of 180 mm. ..... 34
Figure 25: Comparison of the normalized penetration depths from the models with plate radius of 40 mm (Baseline) and 50 mm. ..... 35
Figure 26: Predicted DOP, rod head and plate surface histories with six velocities of rod from the model with target plate radius of 50 mm. ..... 36

# TABLES

Table 1: The parameter values for each test case. ..... 14
Table 2: Material properties used in the analysis..... 16
Table 3: X-FEM simulation results at 1500 m/s for varying mesh resolutions. ..... 22
Table 4: Predicted DOP and P/L with six projectile velocities with polynomial-fit experimental data. (The bold fonts indicate the closest result to the experimental data for each velocity). ..... 27
Table 5: Actual elapsed time for the computer run..... 27
Table 6: Comparison of mesh and boundary for each test case..... 29
Table 7: Predicted DOP and P/L from the model with plate back fixed and free boundary conditions with polynomial-fit experimental data. (The bold fonts indicate the closer result to the experimental data)..... 31
Table 8: Predicted DOP and P/L from the model with target plate thicknesses of 120 mm and 180 mm with polynomial-fit experimental data. (The bold fonts indicate the closer result to the experimental data)..... 33
Table 9: Predicted DOP and P/L from the model with target plate radius of 40 mm and 50 mm with experimental data. (The bold fonts indicate the closer result to the experimental data). ..... 35

# NOMENCLATURE

| | |
|---|---|
| ALE | Arbitrary Lagrangian-Eulerian |
| BC | Boundary Condition |
| DOP, P | Depth Of Penetration |
| EOS | Equation Of State |
| KEOS | "Kerley" Equation Of State |
| L_ROD, L | Rod (projectile) Length |
| MB | MegaByte |
| PIR | Pattern Interface Reconstruction |
| R_PLT | Radius of target PLaTe |
| R_ROD | Radius of ROD (projectile) |
| RHA | Rolled Homogenous Armor |
| S_CEL | Cell Size |
| SR | Density scaling factor ("Scale Rho") |
| SWRI | Southwest Research Institute |
| T_PLT | Thickness of target PLaTe |
| V_ROD, $V_P$ | Rod (projectile) Velocity |
| X-FEM | eXtended Finite Element Method |

# 1. INTRODUCTION

## 1.1. Background

The finite-element shock hydrodynamics code ALEGRA† [18] has recently been upgraded to include an "extended finite element method" (X-FEM) implementation in 2D for simulating impact, sliding, and release between materials in the Eulerian frame [6,19,22,23]. This is a significant extension of the capabilities of ALEGRA and as such requires testing in environments that are representative of the software application space. One application for which ALEGRA is used is high-velocity impact and penetration events. These are inherently multi-material systems which include strong shock waves and high deformations. Often, they require the use of shock-capturing methods, material equation of state (EOS) and constitutive models, and Eulerian meshes with remap algorithms that can maintain the validity of the calculation despite large strains and strain rates.

The problem of long-rod penetration in semi-infinite targets is considered here as representative of one class of impact and penetration events. This problem has been studied in detail in the experiments by Hohler and Stilp (1977,1987) [8,9]. Their experiments involving the impact of long tungsten-heavy-alloy cylinders on plates of hardened steel, reproduced numerically by Anderson, Jr. *et al.* (1991) [3], form a basis for usability testing and validation done in support of ALEGRA code development activities.

In the present report, we describe testing simulations done using ALEGRA with and without the X-FEM capability, in order to evaluate the adequacy of X-FEM for modeling impact and penetration. After a brief description of the numerical methods used in this study, the remainder of the report is organized as follows. Experimental setup and results are discussed briefly in Section 2. The setup for ALEGRA simulations is described in detail in Section 3. Results from these simulations are presented in Section 4, with discussion of post-processing techniques, effects of the mesh setup and resolution, and comparison of results with and without X-FEM to the experimental data.

## 1.2. Numerical methods

ALEGRA is used for all numerical simulations in the present study. ALEGRA is an arbitrary Lagrangian-Eulerian shock hydrodynamics and multi-physics code developed and maintained at Sandia National Laboratories since the 1990's. ALEGRA uses the finite-element method with explicit time integration to solve the equations of solid dynamics for multi-material media subjected to shocks and strong deformations, using material-specific equation of state (EOS) and constitutive models to close the system. ALEGRA also incorporates second-order-accurate interface tracking, remap algorithms that are third-order-accurate in one dimension, modern artificial viscosity methods for handling shock waves, and stabilized "isentropic" multi-material treatment with radiative temperature relaxation [17,18]. ALEGRA validation efforts include the work by Carroll *et al.* (1997) [5] for very similar problems to those considered here: high-velocity impact and penetration of long rods in semi-infinite targets. Other efforts include the

† Arbitrary Lagrangian-Eulerian multi-physics finite-element code for large distortion and shock propagation developed by Sandia National Laboratories.

work by Lemke *et al.* (2005) [14] for magnetically accelerated flyer plates; and Doney *et al.* (2010) [7] for exploding wires, among others.

ALEGRA simulates the motion of material across the domain using the arbitrary Lagrangian-Eulerian (ALE) approach, which moves material with the computational mesh in an initial Lagrangian step, then reconfigures the mesh in a subsequent "remesh" and then a "remap" step. Most commonly, the mesh is reconfigured back to its original, stationary state, which is the Eulerian frame. This remesh and remap operation allows simulations to proceed despite large shear and deformations, but requires the use of advection algorithms to move the solution information between the meshes.

Since Eulerian simulations necessarily generate elements that contain multiple materials, additional infrastructure is required to reconstruct the location and orientation of material interfaces, to partition the deformations to individual materials in an element, and to construct a total element stress based on stresses computed for individual materials in an element. All of these operations introduce significant approximations and errors into the simulations, resulting in spurious behavior in some situations. For example, since the method only allows a single stress and deformation in an element, two materials within an element cannot separate and allow a gap to open when subjected to tensile stresses. Thus the materials are effectively bonded, and only the use of ad hoc modifications to the material state can allow them to separate.

The X-FEM has been implemented in ALEGRA in 2D in order to eliminate these issues, so that inter-material dynamics can be handled as surface phenomena even in the Eulerian frame, without volumetric modifications to the thermodynamic state of the materials. In X-FEM, the finite-element basis functions in each multi-material Eulerian element are "enriched" using Heaviside functions, so that individual materials have basis functions supported only within the region where the material exists. Each material within an element can then have an independent displacement field, with interfaces between them represented explicitly in the solution. With this numerical infrastructure, materials can slide with respect to or separate from one another inside an Eulerian element. The concept of Heaviside enrichment is sketched notionally in Figure 1.

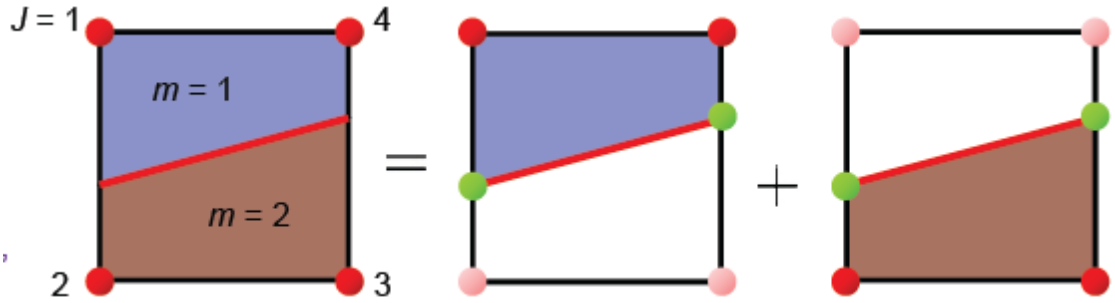


**Figure 1: Heaviside enrichment in X-FEM. Nodes are indexed by *J*, and materials by *m*, within a single element in the computational mesh. Interface intersections are green.**

With the Heaviside enrichment in place, the X-FEM implementation in ALEGRA employs three methods to capture material motion across an Eulerian mesh. First, "pattern interface reconstruction" (PIR) is used to capture material interfaces with maximum fidelity. This method

reproduces linear interfaces in all orientations and has second-order accuracy for planar and curved interfaces (when interface "smoothing" is applied). Second, forces on enriched-element nodes are controlled by a forward-increment Lagrange multiplier contact algorithm which enforces interface physics. This allows inter-material physics to be treated as a true surface phenomenon. Third, remap is performed using a monotonicity-preserving "intersection remap" scheme with third-order limiting, which conservatively remaps materials and material interface intersections from the deformed Lagrangian mesh to the Eulerian mesh.

Although third-order accuracy in intersection remap is available, only the first-order scheme has been fully tested for use in applications, so this scheme is used all simulations shown here. In the standard, "unenriched" ALEGRA formulation, third-order limiting is used by default in single-material regions, but remap uses a "swept-volume" approach, rather than the "intersection" scheme used with X-FEM. In the unenriched formulation only, the order of accuracy used in remap can be controlled directly by the user, and is reduced adaptively by the code when multi-material elements are present in the local stencil. In the *donor* remap configuration, the code uses a first-order-accurate swept-volume scheme for all stencils. In the *aggressive* remap configuration, the code uses up to third-order accuracy, depending on the stencil. Both of these schemes will be used only in unenriched (non-X-FEM) simulations shown here.

With X-FEM, ALEGRA is able to simulate multi-material shock hydrodynamics in the Eulerian frame, while capturing the details of material interface interactions locally. It is anticipated that these methods will dramatically enhance the fidelity with which certain shock-hydrodynamic phenomena can be simulated. For the impact/penetration scenario considered here, ALEGRA's capability using the standard formulation is well established [5]. Thus, our intent is not to characterize any enhancement of fidelity, but to investigate whether ALEGRA still captures the details of classical problems correctly with X-FEM. That is, we aim to show that with X-FEM, results computed using the standard "unenriched" Eulerian methods can still be recovered. To do this, we examine a classical long-rod penetration problem.

## 2. EXPERIMENTAL DATA

The penetration mechanism of long steel- and high-density rods into semi-infinite steel targets of different ultimate yield strength has been investigated experimentally in previous work by Hohler and Stilp (1977, 1987) [8,9] at impact velocities of approximately 500 to 3000 m/s. In the component of Hohler and Stilp's work considered here, all rods were tungsten alloy and circular in cross-section with a length-to-diameter ratio of $L/D = 10$. The calibers varied between $D = 2.5$ to 6 mm, the masses between $m = 1$ to 31 g. The tests were carried out by means of a powder gun and a two-stage light-gas gun. Figure 2 shows the measured penetration depth $P$ normalized by the projectile length $L$ in the "semi-infinite" target as a function of the projectile velocity $V_P$ obtained from the experiment [8,2].

These data appear in Southwest Research Institute (SWRI) Penetration Mechanics Database [2] in Figure 2.1.25, and in the associated data tables in Appendix A (pages A-119 to A-124, from the "Hohler and Stilp (1991a)" section). The data used here were extracted for the $L/D = 10$ case, where right circular cylinders were shot at normal incidence. The data do not include any information on measurement uncertainty or other potential sources of error, and no attempt was

made here to quantify the errors. An inherent variability of a few percent is apparent. These experiments have been simulated previously using many other codes, with comparison to experimental data, as shown by Anderson, Jr. *et al.* (1991) [3] and Templeton *et al.* (2002) [21], among others. The experiments have not been simulated previously using any X-FEM implementation.

The projectile material is the "D17.6" tungsten alloy: ambient density 17,600 kg/m$^3$ and Brinell hardness number 406 [2]. The target material is the "HzB,A" armor steel: ambient density 7,850 kg/m$^3$ and Brinell hardness number 255 [2]. These results and others from experiments very similar to these appear – in graphical form only – in Hohler and Stilp (1977, 1987) [8,9]. The D17.6 tungsten alloy was used also in the time-resolved penetration experiments of Anderson *et al.* (1995) [1], who describe it as a sintered alloy with the composition 92.5% W, 4.85% Ni, 2.4% Fe, 0.25%Co. The HzB,A material is a high-hard armor steel, but the details of its composition are unknown. In the original experiments, it is not clear how the penetration depth was measured, but unpublished documents from Ernst Mach Institute indicate that this type of experiment typically used post-test sectioning of the target plates and direct measurement of the penetration channel depth relative to the original surface plane. (The later experiments of Anderson *et al.* (1995) [1] used time-resolved x-ray imaging.) Hohler and Stilp (1977, 1987) note that the "S-shape" of the penetration trend versus impact velocity is a consequence of the hydrodynamic character of the penetration event at higher impact velocities [8,9], and indicates the "dynamic strength" of the target material exceeds that of the projectile material.

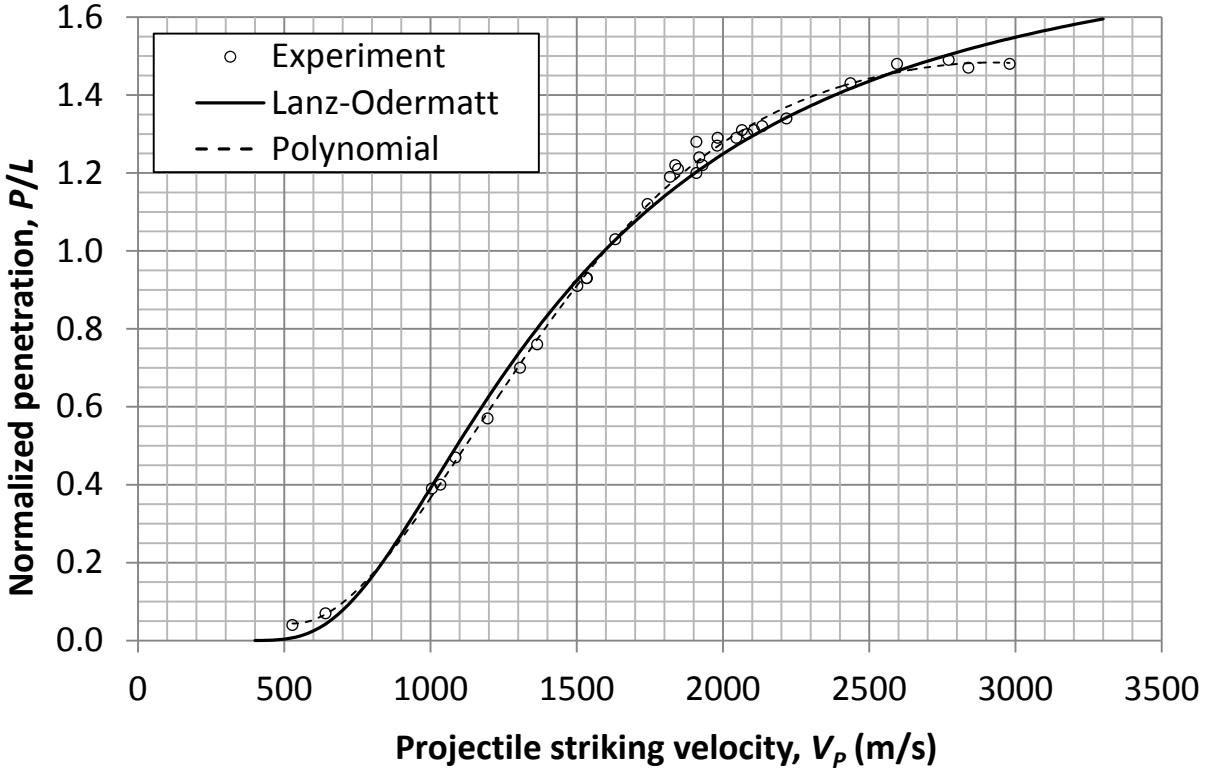


**Figure 2: Experimental data from a penetration mechanics database [2]: the penetration depth *P* normalized by the projectile length *L* as a function of the projectile velocity $V_P$, with empirical data fits based on the Lanz-Odermatt formula [13] and a 5th-order polynomial.**

A semi-analytical empirical fit to Hohler and Stilp's data is included in Figure 2, based on the commonly used inverse-exponential form originally devised by Lanz and Odermatt (1992) [13] for long-rod penetration in semi-infinite targets, as modified by Rapacki *et al.* (1995) [15]:

$$\frac{P}{L} = a\sqrt{\frac{\rho_P}{\rho_T}}\, e^{-\left(\frac{2S}{\rho_P V_P^2}\right)} \tag{1}$$

In this formula, the target material penetration resistance is represented by the quantity

$$S = k(BHN)^M \tag{2}$$

which has units of stress. The projectile and target ambient densities are denoted by $\rho_P$ and $\rho_T$, respectively, and the Brinnell hardness of the target material by $BHN$. In these formulae, the quantities $a$, $k$, and $M$ are obtained by a least-squares fit of the formulae to the experimental data. The asymptotic normalized penetration at very high velocities is represented by the "hydrodynamic multiplier," $a$. The exponent in the formula represents the ratio of material penetration resistance to projectile dynamic pressure. (See also Reference 20.)

For the "Lanz-Odermatt" fit shown in Figure 2 and elsewhere in this report, the target hardness is assumed to be $BHN$ = 295, which is the mean value in the range quoted by Hohler and Stilp (1977) [8], rather than the value quoted in the Penetration Mechanics Database [2]. Least-squares fitting to the data yields the following fit parameters: $a$ = 1.22817, $k$ = 1.63084 GPa, and $M$ = 0.373287. These values compare favorably with the values obtained by Rapacki *et al.* (1995) [15] for similar materials in a separate set of experiments. However, the fit fails to capture data points accurately at the extrema of the velocity range, and slightly diminishes the slope of the curve. Therefore, a purely empirical fit is also included using a simple 5$^{th}$-order polynomial.

## 3. MODEL DESCRIPTION

For validation testing of X-FEM in ALEGRA, simulations for the test cases in Table 1 were conducted. The depths of penetration (DOP = $P$), with six rod velocities (V_ROD = $V_P$), for each case were calculated as a result from an ALEGRA run. Each DOP was normalized by the original length of the projectile (L_ROD = $L$). The normalized penetration depths ($P/L$) with V_RODs for the baseline model were compared to the experimental data.

Figure 3 shows the schematic diagram of the model and boundary conditions (BC). The target plate thickness (T_PLT) and radius (R_PLT) for the baseline are 120 mm and 40 mm, respectively. The projectile rod length (L_ROD) and radius (R_ROD) for the baseline are 50 mm and 2.5 mm, respectively. To investigate the model parameter effect, the boundary condition on the plate back surface, T_PLT, and R_PLT were changed as listed in Table 1, using either a free-

motion (unconstrained) condition, or a "no-displacement" condition, which prevents motion normal to the boundary. The denotation of each parameter in Table 1 is shown in Figure 3.

**Table 1: The parameter values for each test case.**

| Test case | Rod radius, R_ROD (mm) | Rod length, L_ROD (mm) | Plate radius, R_PLT (mm) | Plate thickness, L_PLT (mm) | BC on Plate Back Surface |
|---|---|---|---|---|---|
| 4x12fixed | 2.5 | 50. | 40. | 120. | No displacem't |
| 4x12free | 2.5 | 50. | 40. | 120. | Free |
| 4x18fixed | 2.5 | 50. | 40. | 180. | No displacem't |
| 5x12fixed | 2.5 | 50. | 50. | 120. | No displacem't |

Note: 4x12fixed is the baseline.

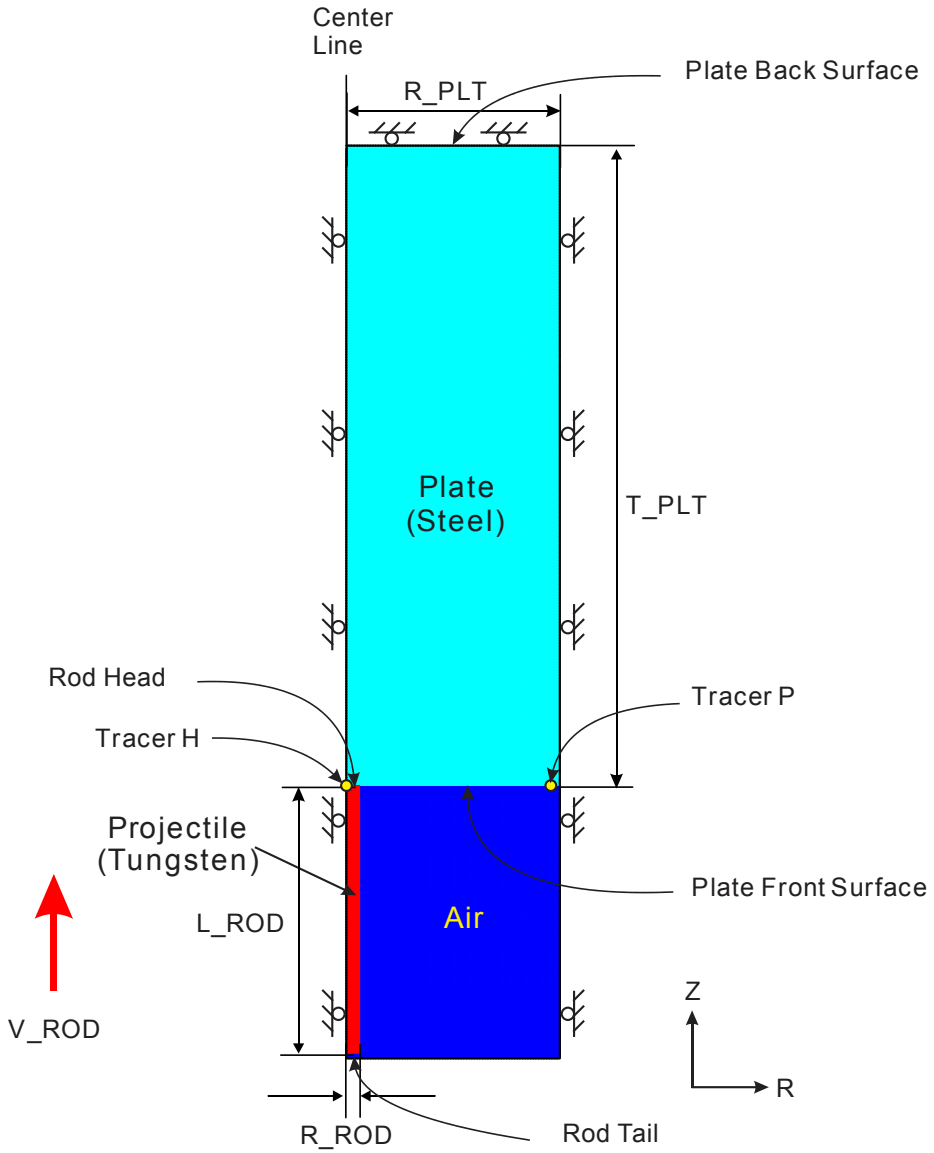


**Figure 3: Schematic diagram and boundary conditions of the model with denotation of each parameter.**

Making use of axisymmetry, only a half-section of the target plate and the rod projectile are modeled as shown Figure 3. The projectile moves from bottom to top, in the +$z$-direction. The left boundary is the axis of axisymmetry. A zero-displacement boundary condition (radial direction) is applied on the right boundary of the model to represent the "semi-infinite" steel target. A zero-displacement boundary condition (axial direction) is applied on the upper boundary to better represent the projectile impact conditions in the experiments for the baseline model.

The BC's and dimensions of the target were chosen to represent impact and penetration in a semi-infinite target. The actual dimensions of the experimental target are unknown, but all of the data are categorized in the Penetration Mechanics Database under "Semi-Infinite Data" [2], meaning that the target plate was large enough to stop all projectile impacts for the given velocities, without spall or breakout on the rear surface. Since we cannot model the entire dimensions of the real plate, we must model the semi-infinite effect as best we can using a plate of finite dimensions and fixed or free boundary conditions. The purpose of the runs listed in Table 1 was to identify which set of target dimensions and BC's most accurately represents the semi-infinite system.

The equation of state (EOS) material properties for the projectile rod and target plate were obtained from Sesame tabular libraries, using the "KEOS" (Kerley) interface in ALEGRA, as listed in Table 2. The KEOS Sesame model is an implementation of the Sesame EOS in ALEGRA. The KEOS Sesame model uses the same tables that are used by the CTH‡ SES model. The von Mises flow stress model is used for the yield calculation. The model for the von Mises flow stress, $\sigma$, is the form of Johnson and Cook (1983) [10]:

$$\sigma = [A + B\epsilon^n][1 + C \ln \dot{\epsilon}^*][1 - T^{*m}] \tag{3}$$

where $\epsilon$ is the equivalent plastic strain, $\dot{\epsilon}^* = \dot{\epsilon}/\dot{\epsilon}_0$ is the dimensionless plastic strain rate for $\dot{\epsilon}_0 = 1.0\ \mathrm{s}^{-1}$, and $T^*$ is the homologous temperature, which quantifies the departure from the melt temperature $T_M$. The quantities *A, B, n, C*, and *m* are material constants obtained empirically for common materials. The expression in the first set of brackets gives the stress as a function of strain for $\dot{\epsilon}^* = 1.0$ and $T^* = 0$. The expressions in the second and third sets of brackets represent the effects of strain rate and temperature, respectively. The Johnson-Cook model parameters used in ALEGRA in this study are shown in Table 2.

The yield model and parameters used here are those used in CTH and EPIC by Templeton *et al.* (2002) [21]. As these parameters were used successfully in this previous work (<10% deviation from Hohler and Stilp's data), they were used again here. However, no conclusive evidence exists which establishes any certain combination of material response models for this problem as the most accurate. The tabular Sesame EOS models are used here, rather than the analytic Mie-Grüneisen EOS models used previously. Other successful parameter settings for this problem or similar problems and materials can be found in Kmetyk and Yarrington (1988) [12]; Anderson, Jr. and Walker (1991) [3]; Anderson, Jr. *et al.* (1995) [1]; and Carroll *et al.* (1997) [5].

‡ CTH is a multi-material, large deformation, strong shock wave, solid mechanics code developed at Sandia National Laboratories.

**Table 2: Material properties used in the analysis.**

| | Input Parameter | Unit | Projectile Rod (Tungsten) | Target Plate (HzB, Steel) |
|---|---|---|---|---|
| KEOS Model | FEOS | - | SESAME | SESAME |
| | NEOS | - | 3550 | 2150 |
| | Density (ρ) | $kg/m^3$ | 17760 | 7850 |
| | SR | - | 1.094 | 1.003 |
| Yield Model (Johnson-Cook) | *A* | GPa | 1.365 | 0.810 |
| | *B* | GPa | 0.1765 | 0.5095 |
| | *C* | - | 0.016 | 0.014 |
| | *m* | | 1.00 | 1.030 |
| | *n* | | 0.12 | 0.260 |
| | $T_M$ | K | 3695 | 1818 |
| | Poisson ($\nu$) | - | 0.281 | 0.299 |

Note: - KEOS stands for "Kerley" EOS. KEOS is an interface to Sesame data that was built by Gerald Kerley and is very commonly used in ALEGRA simulations.
- SR is a density scaling factor, which represents the ratio of molecular weight for the table relative to the actual material. For alloys it is commonly used to relate the pure material density to the alloy density.

# 4. ANALYSIS RESULTS

## 4.1. Depth of penetration

To calculate the depth of penetration (DOP) from ALEGRA simulations, Lagrangian "Tracers" H and P were placed at the center of the rod nose or "head" and at the edge of the target or "plate" front surface, respectively, as shown in Figure 3. "Tracers" are diagnostic markers used to track material or mesh motion locally in an ALEGRA calculation. Lagrangian tracers are advected with the medium by interpolation of the velocity field. Figure 4 shows the *z*-positions of Tracers H ("rod head") and P ("plate surface") as a function of time from the baseline model with V_ROD=3000 m/s as an example. Figure 5 presents views of progression of the formation of the penetration channel at 0 and 49 μs. We observe that the rod nose/head position goes through a maximum, and subsequently recoils. Also, the plate surface near the penetration channel moves downward (-*z*-direction) as the rod head moves into the target, due to crater formation. The plate surface position at the outer radius continues to oscillate through the duration of the simulation.

To mimic a post-test penetration measurement, DOP data extracted from the ALEGRA simulations must use the maximum *z*-position reached by the rod head, and some representation of the final *z*-position of the plate surface, after oscillations have damped out. To approximate this, we take the perpendicular distance between the positions of rod head (Tracer H) and the plate front surface (Tracer P) at the time of maximum Tracer-H *z*-position to be the DOP. (Continuing the simulation until plate oscillations damp out would be prohibitively expensive.) In the V_ROD=3000 m/s case shown in Figure 4, the positions of rod head and plate surface are calculated to be 74.5 mm and -1.8 mm, respectively, at 49 μs (time at the peak of the Tracer H curve). Thus, the DOP is calculated to be 76.3 mm.

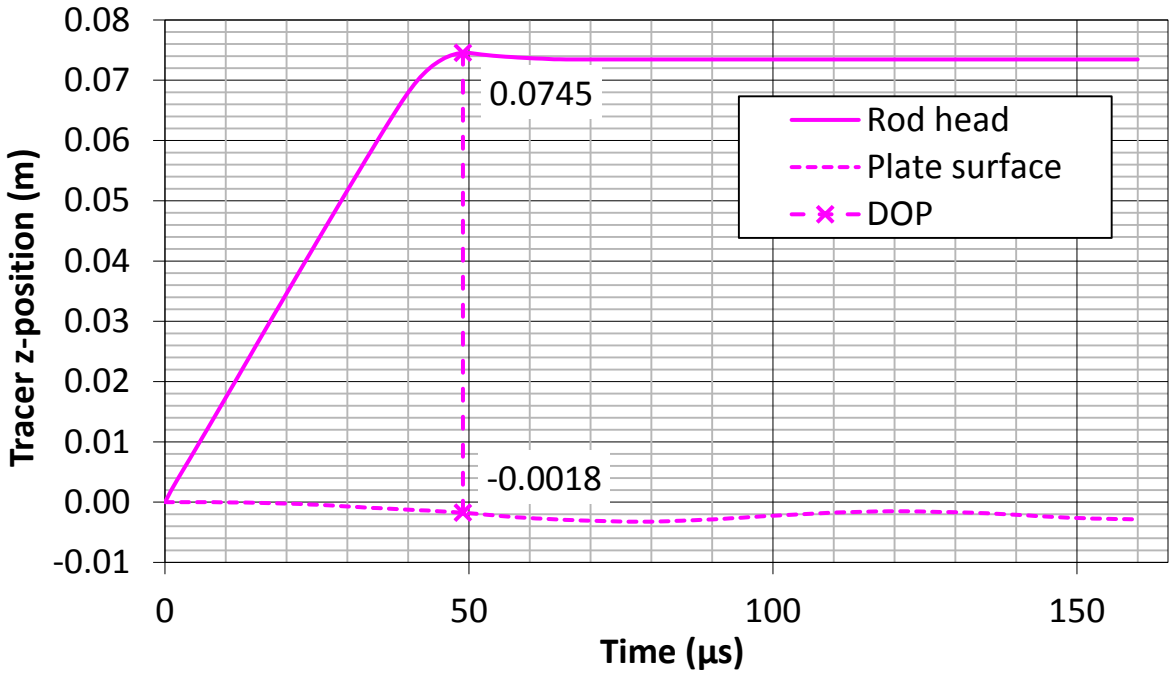


**Figure 4: Calculation of DOP for the baseline case with V_ROD=3000 m/s.**

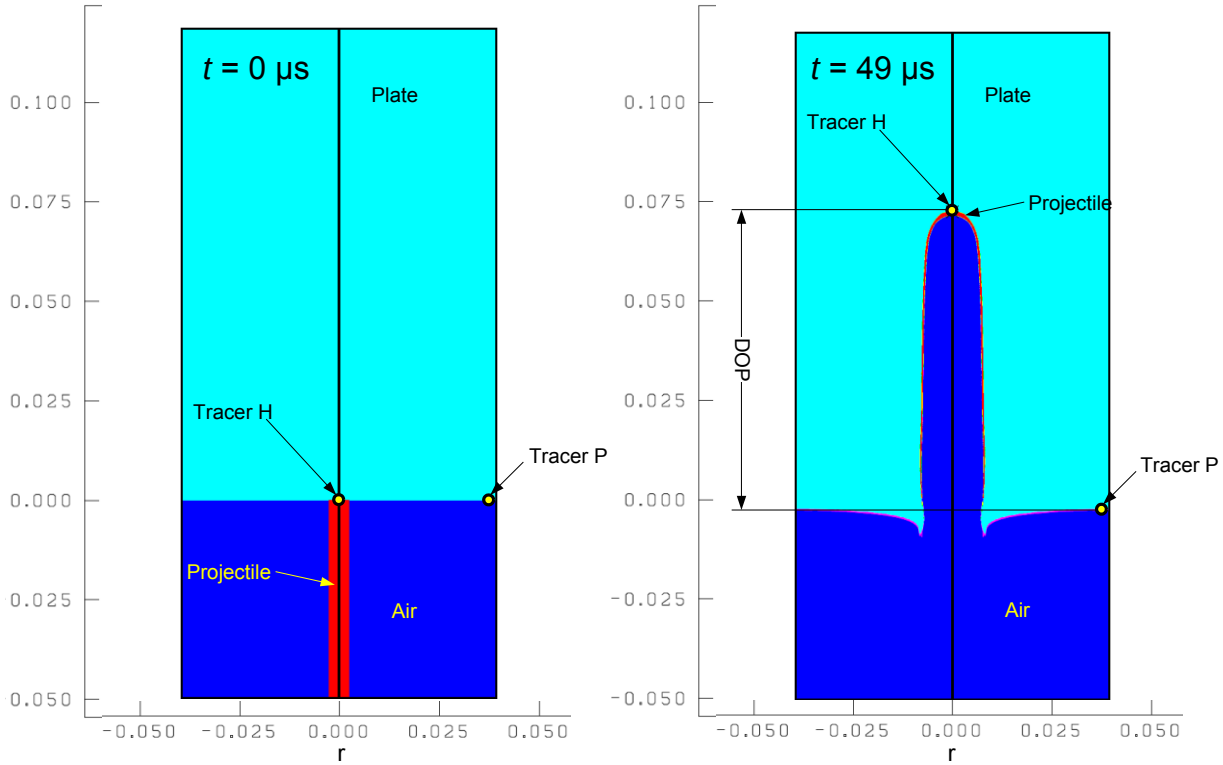


**Figure 5: Simulation results at 0 and 49 µs for the baseline case with V_ROD=3000 m/s (Unit on axes is m).**

## 4.2. Mesh resolution

Use of the X-FEM algorithm in ALEGRA instead of the standard Eulerian formulation incurs dramatically increased computational cost. The mesh with a smaller cell size provides higher accuracy, but spends more computer running time. Therefore, an appropriate mesh cell size and configuration must be determined. To examine the cell size effect on the accuracy of the analysis result and the computer running time, meshes with various cell size are constructed, shown in Figure 6 through Figure 11. The DOPs are calculated from the ALEGRA solutions using these meshes, with and without X-FEM. The geometries of the baseline (4x12fixed) in Table 1 and material properties in Table 2 are used as input parameter values. A projectile velocity of 1500 m/s is used for all cases for comparison purposes. The ALEGRA runs are performed using 64 nodes (512 processors) on RedSky[§].

The meshes in Figure 6 through Figure 8 were generated using ALEGRA's inline meshing capability, as uniform meshes. The cell sizes in the *x*- and *y*- directions are the same as the input cell size value. The projectile rod head is expected to move between 0 mm to 78 mm on the center line of the model since the penetration depth was measured as 74.1 mm for the projectile velocity of 3000 m/s (maximum velocity in this study) [2]. The crater radius is expected to be less than four times the projectile rod radius. The region $0 \leq z \leq 78$ mm and $0 \leq r \leq 10$ mm is defined as the "penetration area". The same size of cells in the outside and inside of the penetration area is inefficient for the computer run. The graded cell size meshes as shown Figure 9 through Figure 11 were generated using the programmable cell size options in ALEGRA's inline mesh capability. Cells smaller than the input cell size value (S_CEL) were generated in the penetration area. In the 5-G subcase, the cell size input value of 0.15 mm generated the cell sizes of 0.05 mm and 0.07 mm in the *r*- and *z*- directions. The cell size gradually increases outside the penetration area. The number of elements in 5-G mesh is smaller than that of 3-U mesh while the cell size for the 5-G subcase in the penetration area is smaller than that of subcase 3-U: *i.e.*, subcase 5-G will produce more accurate results with fewer elements than subcase 3-U, due to the graded mesh.

§ Red Sky is a platform which is assembled in the space where the legendary system ASCI Red once stood at Sandia National Laboratories.

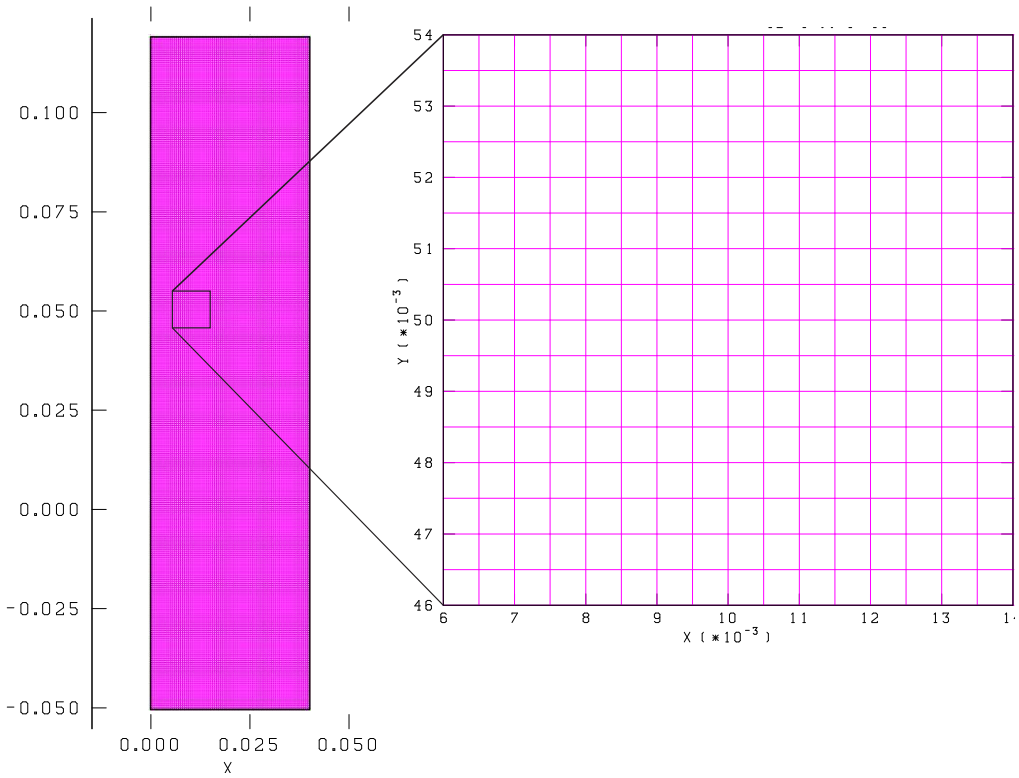


**Figure 6: Computational mesh for uniform cell size=0.5 mm (Unit on axes: m).**

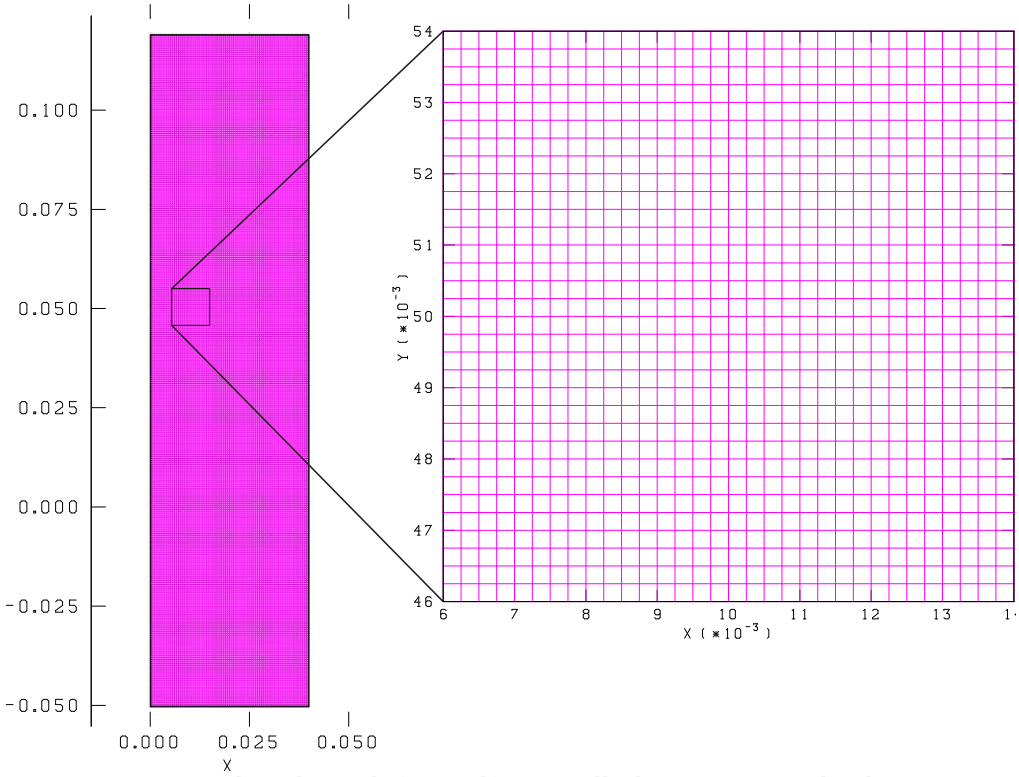


**Figure 7: Computational mesh for uniform cell size=0.25 mm (Unit on axes: m).**

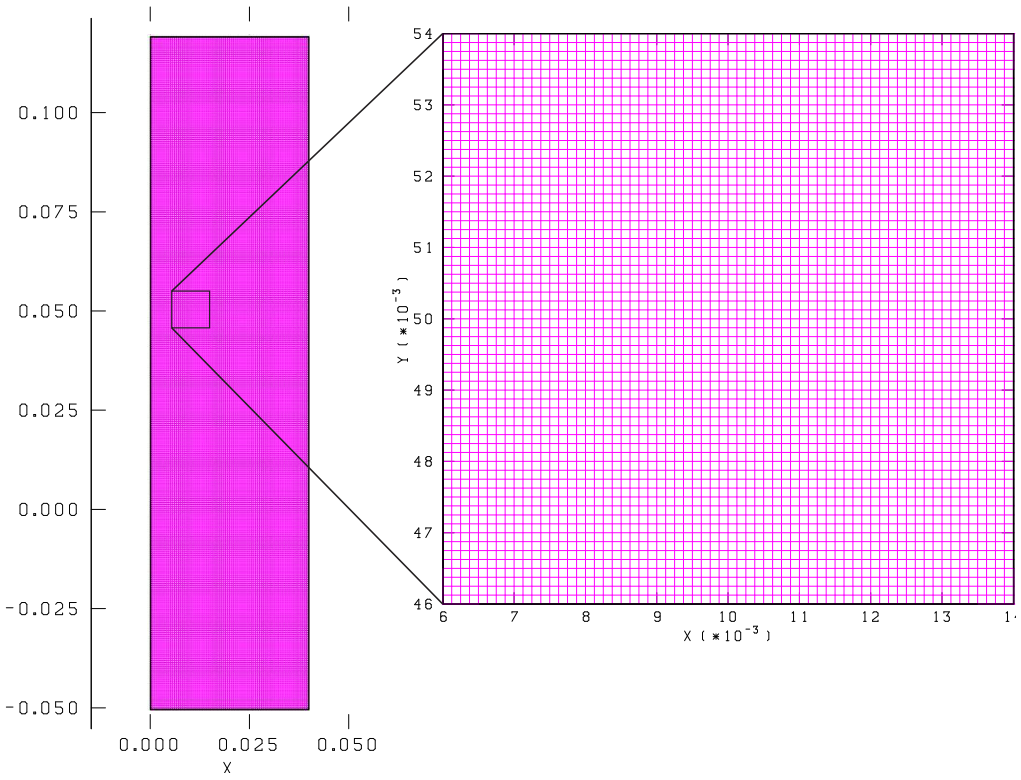


**Figure 8: Computational mesh for uniform cell size=0.125 mm (Unit on axes: m).**

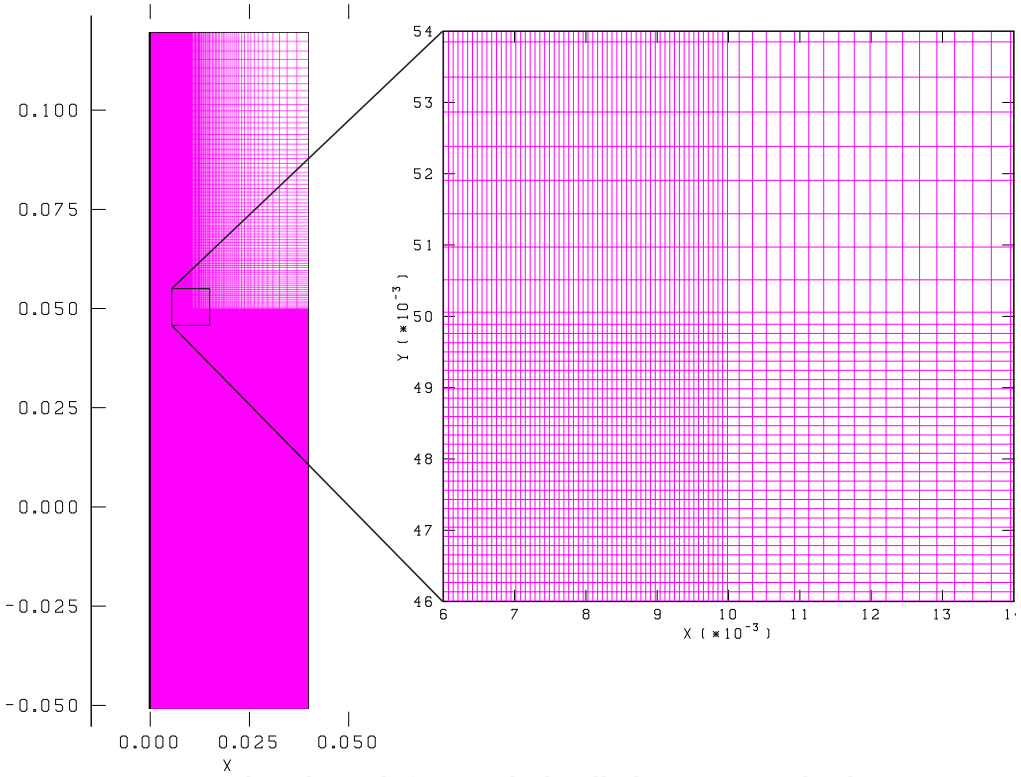


**Figure 9: Computational mesh for graded cell size=0.2 mm (Unit on axes: m).**

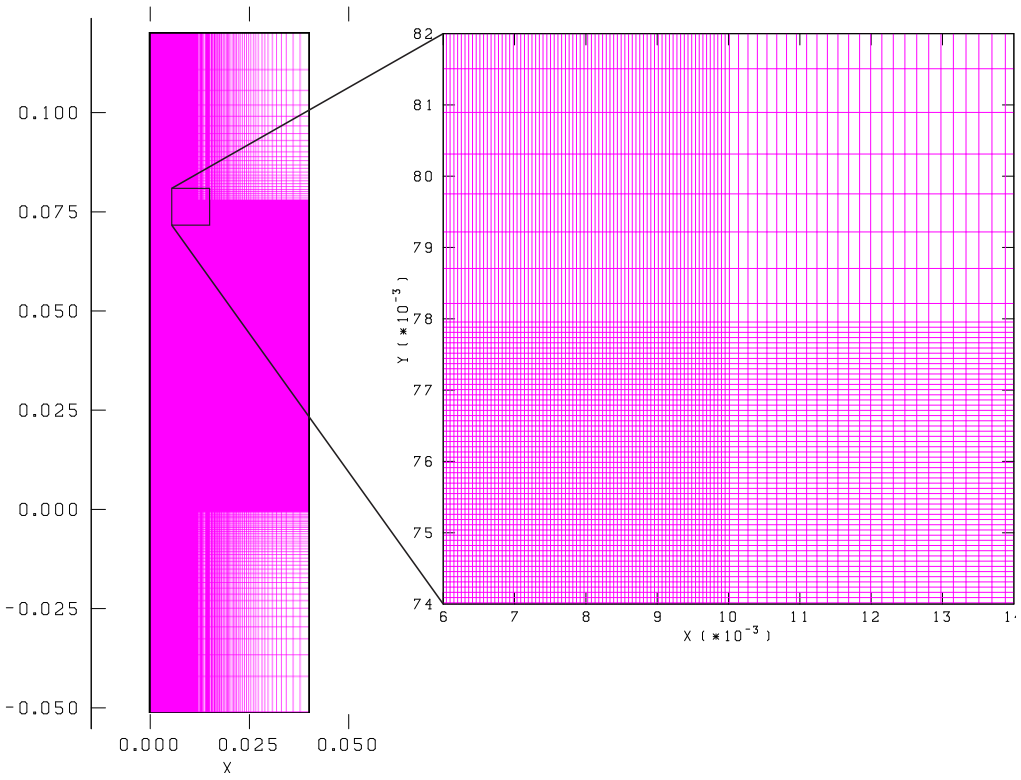


**Figure 10: Computational mesh for graded cell size=0.15 mm (Unit on axes: m).**

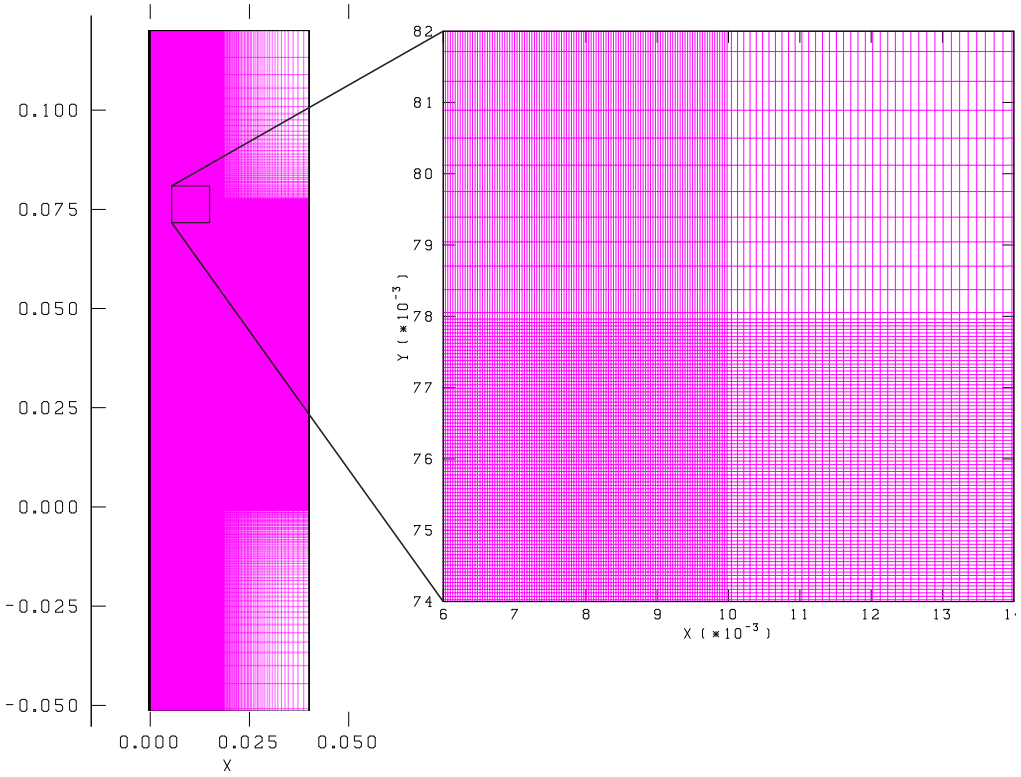


**Figure 11: Computational mesh for graded cell size=0.1 mm (Unit on axes: m).**

A series of simulations was performed at varying mesh resolution for 1500-m/s impact, using both ALEGRA's X-FEM and standard "unenriched," or "U-FEM" methods. Uniform and graded meshes were used to achieve the desired mesh resolution in the penetration region. Table 3 lists the mesh type, cell size, number of elements, size of EXODUS II** file as an output, actual elapsed time for each of the X-FEM computer runs, and calculated DOP for each mesh.

**Table 3: X-FEM simulation results at 1500 m/s for varying mesh resolutions.**

| Subcase | Type | Input cell size, S_CEL (mm) | Cell size in penetration area (mm) | | | No. of elements | EXODUS File Size (MB) | Elapsed time (hh:mm:ss) | Predicted DOP (mm) | Figure |
|---|---|---|---|---|---|---|---|---|---|---|
| | | | $\Delta r$ | $\Delta z$ | $h$ | | | | | |
| 1-U | Uniform | 0.5 | 0.5 | 0.5 | 0.5 | 27280 | 375 | 00:27:21 | 38.134 | Figure 6 |
| 2-U | Uniform | 0.25 | 0.25 | 0.25 | 0.25 | 109280 | 1500 | 00:44:54 | 41.895 | Figure 7 |
| 3-U | Uniform | 0.125 | 0.125 | 0.125 | 0.125 | 437440 | 6028 | 02:23:38 | 43.696 | Figure 8 |
| 4-G | Graded | 0.2 | 0.067 | 0.129 | 0.098 | 170800 | 2355 | 02:15:36 | 44.004 | Figure 9 |
| 5-G | Graded | 0.15 | 0.052 | 0.073 | 0.063 | 301644 | 3316 | 04:09:38 | 44.546 | Figure 10 |
| 6-G | Graded | 0.1 | 0.035 | 0.049 | 0.042 | 680000 | 5852 | 08:20:08 | 44.825 | Figure 11 |

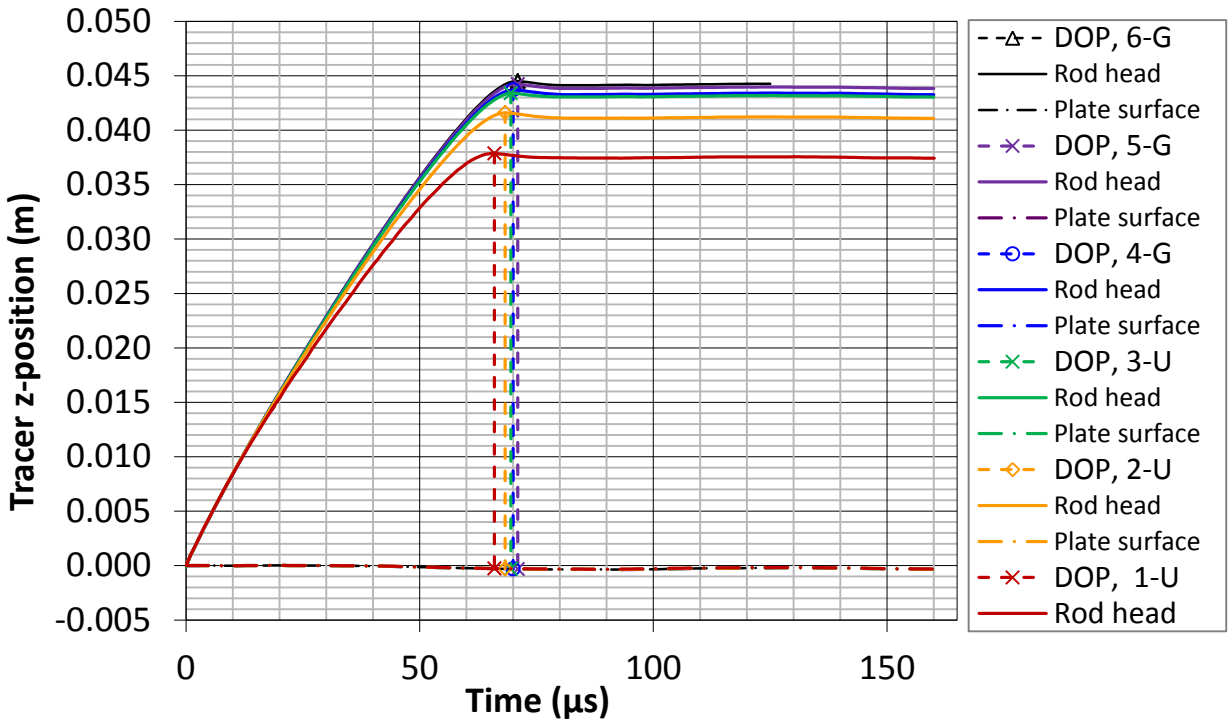


**Figure 12: Predicted DOP, rod head and plate surface histories with VP=1500 m/s from X-FEM simulation using the mesh with various cell sizes.**

** EXODUSII is a file format developed to store and retrieve data for finite element analyses. It is used for pre-processing (problem definition), post-processing (results visualization), as well as code-to-code data transfer. An EXODUS II data file is a random access, machine independent, binary file that is written and read via C, C++, or FORTRAN library routines which comprise the Application Programming Interface (API).

As described above, transient penetration data for each of these simulations were obtained using curves of rod nose/head (Tracer H) and plate surface (Tracer P) for the subcases. These histories are shown graphically in Figure 12. The data indicate that as the mesh is refined, the DOP and time of DOP both increase, but are convergent. The motion of the front plate contributes relatively little to the DOP.

These data are rearranged and overlaid on the experimental data and fits in Figure 13, which shows the calculated normalized penetration depths ($P/L$) obtained using ALEGRA with X-FEM for the projectile velocity of 1500 m/s from the meshes with various cell sizes. Table 3 lists the mesh type, cell size, number of elements, size of EXODUS II file as an output, actual elapsed time for each of the X-FEM computer runs, and calculated DOP for each mesh. The characteristic element dimension shown in Table 3 for uniform and graded meshes is given by $h = (\Delta r + \Delta z)/2$.

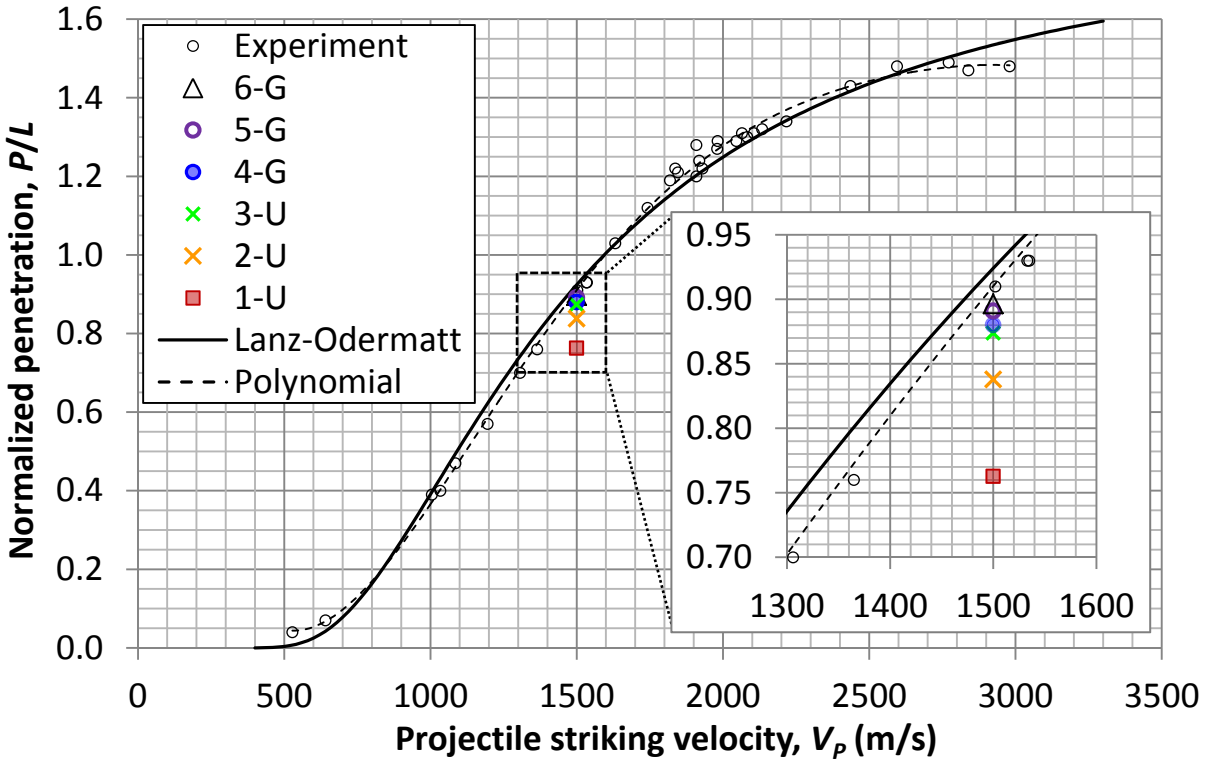


**Figure 13: Depths of penetration with $V_P$=1500 m/s from X-FEM simulation using the mesh with various cell sizes.**

We see qualitatively that the DOP increases toward the experimental results as the mesh is refined. To quantify this convergence trend, the following technique is used, based on the "multi-regression" technique of Rider and Kamm (2012) [16] and Kamm *et al.* (2012) [11]. We begin by postulating that the simulated DOP data can be represented in the form $P = a + bh^c$, which appears as Equation 15 in Reference 16. Least-squares fitting of this expression to the simulation results is used to infer both an intrinsic convergence rate and an asymptotic "converged" value of $P$. The rate appears as $c$ in this expression, and the converged value is $a$. The least-squares fit produces estimates for these values, given the simulation DOP data.

Uncertainty bounds on the convergence rate are obtained by assuming an error of $\pm h$ in the DOP value. We define upper and lower bounds on the simulated $P$ values as $P_+ = P + h$ and $P_- = P - h$, and then repeat the least-squares fit for $P_+$ and $P_-$ each as a function of $h$. This provides uncertainty bounds on the inferred convergence trend.

This technique yields the three curves shown in Figure 14. Since the convergence trend is smooth and monotonic, the "screening" recommended by Rider and Kamm (2012) [16] is not needed. The inferred mean convergence rate is $c = 1.061$, with an uncertainty of +0.005/-0.004. The X-FEM results thus demonstrate extremely tight adherence to a smooth, monotonic, first-order convergence trend, as expected for this class of problems. Furthermore, the "converged" value of $P$ produced by this analysis is $a = 45.33$ mm. Evaluating the polynomial fit shown in Figure 2 at $V_p$=1500 m/s yields a reference experimental DOP of 45.42 mm. The converged X-FEM simulation result therefore differs from the experimental expectation by only 0.2%. Very similar convergence behavior was obtained for U-FEM results as well (not shown here).

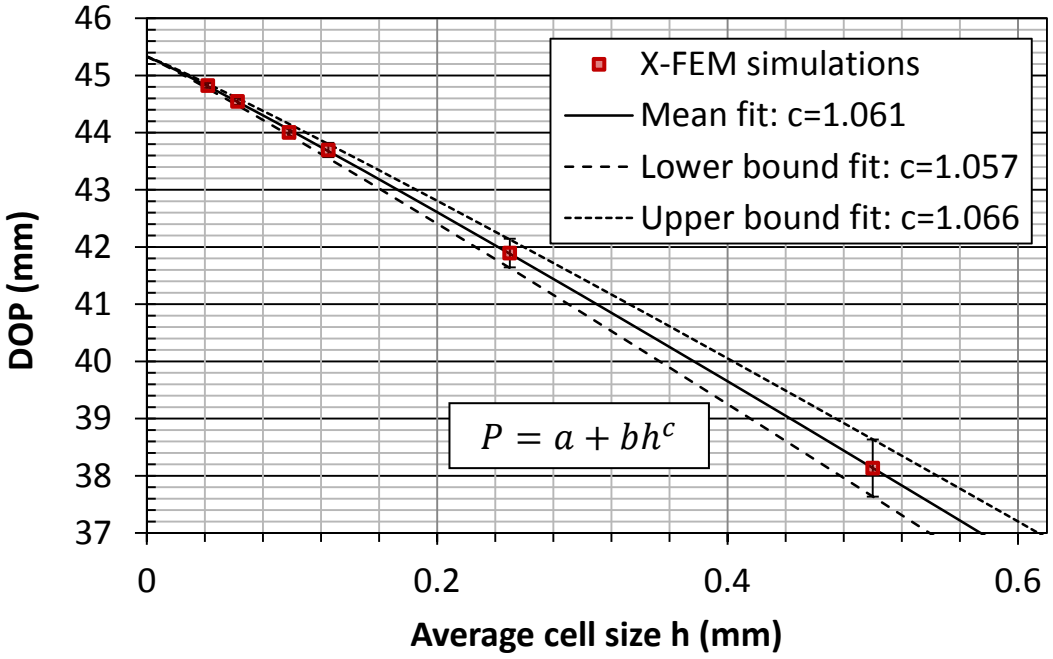


**Figure 14: Mesh sensitivity for X-FEM and standard ALEGRA ("U-FEM") results.**

It should be noted that the simulation for an input cell size of 0.1 mm (6-G) ended after 125 μs, as can be seen by examination of Figure 12. Failures such as this persist but only affect a relatively small number of X-FEM simulations (see Sections 4.4.1-4.4.3). Since the X-FEM implementation is very recently developed, it is anticipated that ongoing and future work will improve the robustness, stability, and performance of ALEGRA simulations with X-FEM.

Due to the large costs and risk of simulation stopping involved with the finest mesh (6-G), the remainder of this study was conducted using the graded cell size of 0.15 mm as the most appropriate and expedient mesh configuration (5-G, average cell dimension in penetration area: $h$ = 0.063 mm). This is the only configuration which allows runtimes under 5 hours and DOP at 1500 m/s within 2% of the converged value.

## 4.3. Comparison to the standard finite-element algorithms

For validation testing purposes, DOPs are calculated using X-FEM simulations for projectile velocities of 500, 1000, 1500, 2000, 2500, and 3000 m/s, with the baseline model (4x12fixed) and the 5-G subcase. Figure 15 shows the Tracer H (rod head) and Tracer P (plate surface) histories for six velocities of projectile. The DOPs are predicted to be 1.98, 17.18, 44.55, 63.47, 71.95, and 76.31 mm for the projectile velocities of 500, 1000, 1500, 2000, 2500, and 3000 m/s, respectively. The predicted DOPs normalized by the projectile length are very close to the experimental data as shown Figure 16.

For comparison purposes, the DOPs are calculated using *aggressive* and *donor* advection in the standard ALEGRA "unenriched" finite element formulation. Henceforward, the standard unenriched formulation will be referred to as "U-FEM." Table 4 and Figure 17 summarize the results from three simulations with the polynomial fit to the experimental data. The X-FEM algorithm yields the closest DOP to the data when the projectile velocity is 3000 m/s, while the U-FEM *aggressive* algorithm yields the closest DOP for projectile velocities of 1000, 1500, 2000, and 2500 m/s; and the *donor* algorithm yields the closest DOP for projectile velocity of 500 m/s.

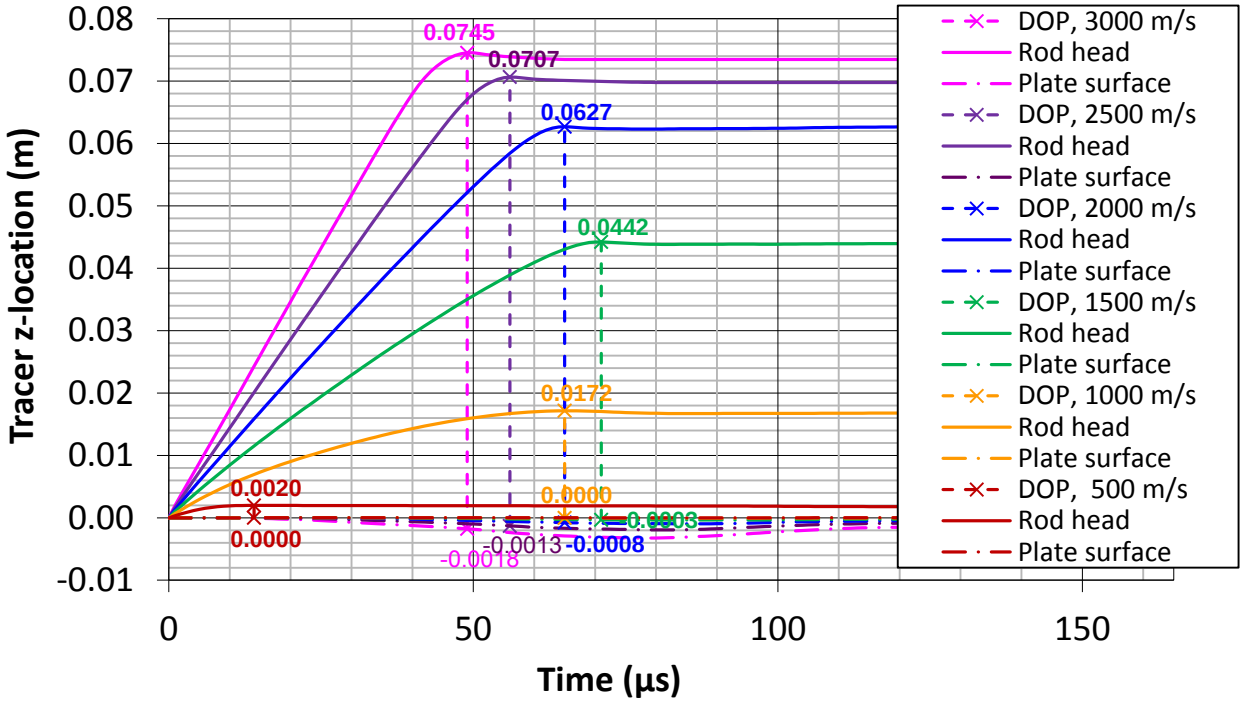


**Figure 15: Predicted DOP, rod head and plate surface histories from X-FEM with six velocities of rod.**

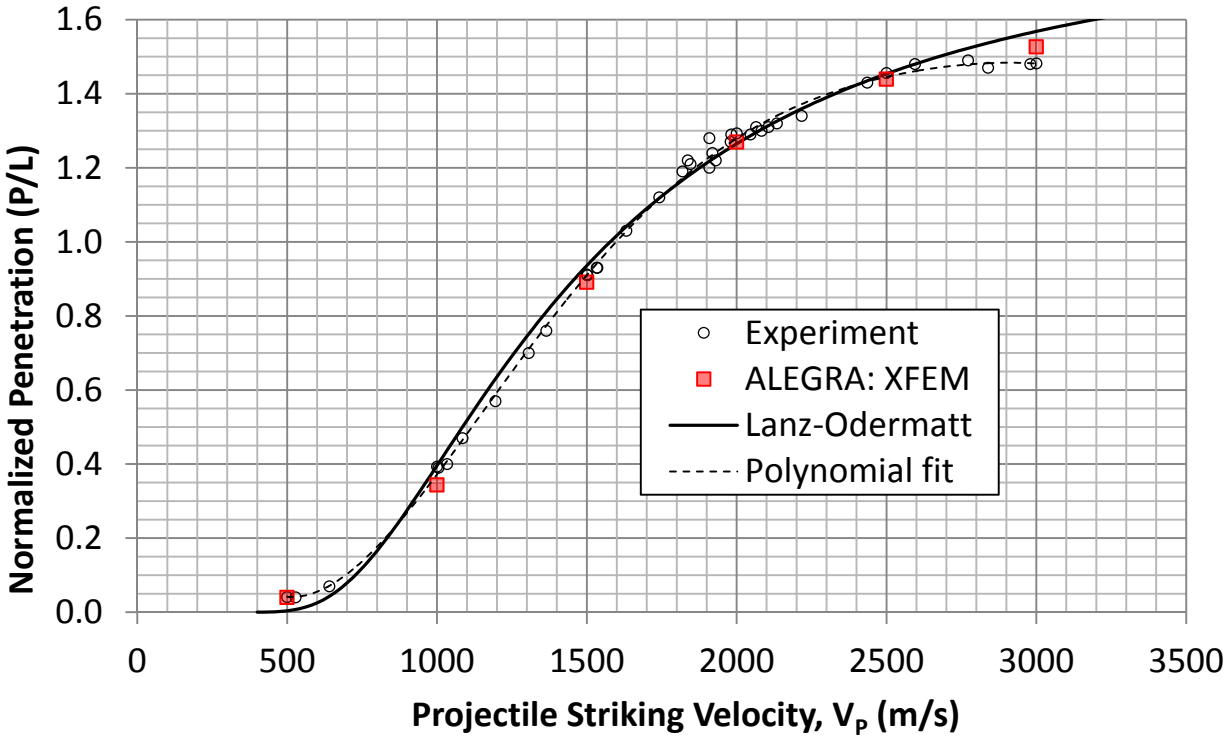


**Figure 16: Comparison between the experimental data with predicted normalized penetration depths from X-FEM simulation.**

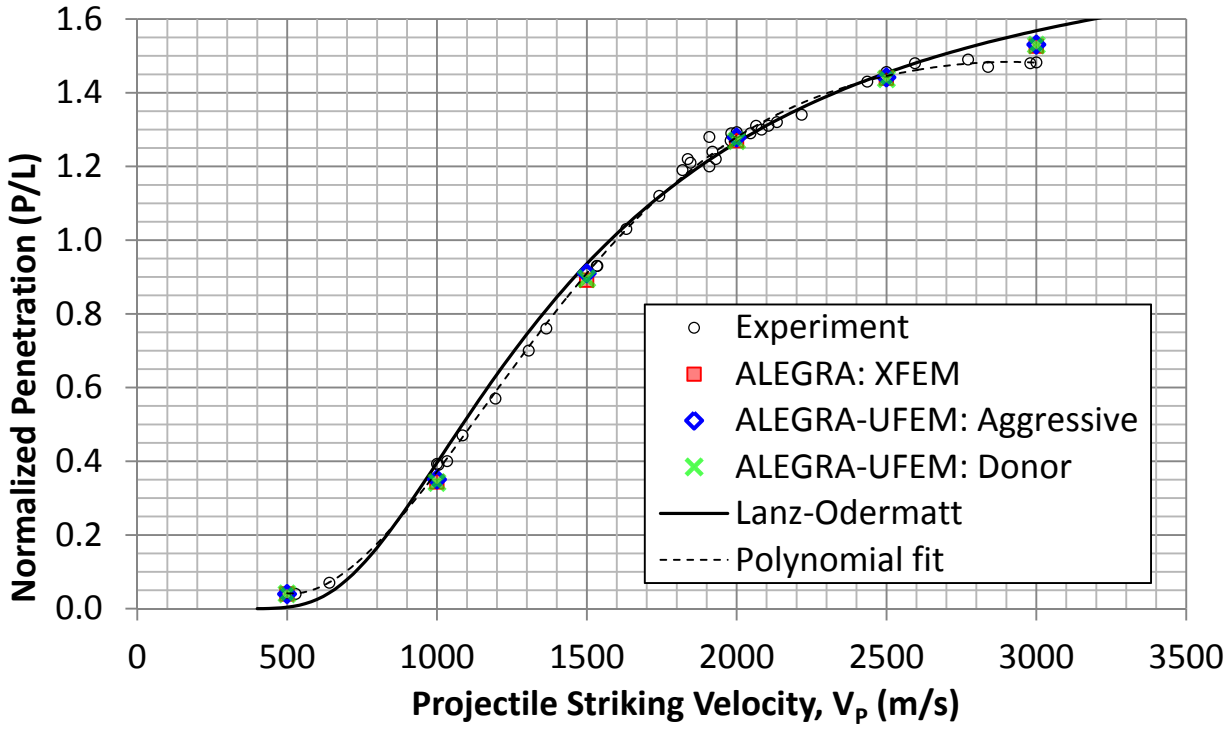


**Figure 17: Comparison between the predicted normalized penetration depths from X-FEM, *aggressive* and *donor* aggressive simulations, and experimental data.**

In general, all three algorithms compare very favorably to the experimental data. When computed in terms of mean difference in *P*/*L* for all six velocities, the X-FEM data differ from the polynomial fit to experimental data by 1.58%. They differ from the U-FEM aggressive results by 0.51%. The U-FEM *aggressive* results differ by 1.40% from the experimental *P*/*L* polynomial fit, and the U-FEM *donor* results by 1.62%. These differences (shown in Table 4) are well within any plausible measurement uncertainty that may be assumed to be inherent to the experimental data. It is interesting to note that the penetration depths increase toward the experimental data as the remap method in U-FEM is changed from *donor* (first-order) to *aggressive* (third-order). The "intersection remap" algorithm used in this study for the X-FEM simulations in this study is only first-order, as noted in Section 1.2.

**Table 4: Predicted DOP and P/L with six projectile velocities with polynomial-fit experimental data. (The bold fonts indicate the closest result to the experimental data for each velocity).**

| Projectile Velocity (m/s) | X-FEM | | UFEM, *aggressive* | | UFEM, *donor* | | Data (polynomial fit) | |
|---|---|---|---|---|---|---|---|---|
| | DOP (mm) | P/L | DOP (mm) | P/L | DOP (mm) | P/L | DOP (mm) | P/L |
| 500 | 1.98 | 0.040 | 1.96 | 0.039 | **1.98** | **0.040** | 2.07 | 0.041 |
| 1000 | 17.18 | 0.344 | **17.52** | **0.350** | 17.10 | 0.342 | 18.55 | 0.371 |
| 1500 | 44.55 | 0.891 | **45.48** | **0.910** | 44.73 | 0.895 | 45.42 | 0.908 |
| 2000 | 63.47 | 1.269 | **63.90** | **1.278** | 63.48 | 1.270 | 63.82 | 1.276 |
| 2500 | 71.95 | 1.439 | **72.08** | **1.442** | 71.87 | 1.437 | 72.06 | 1.441 |
| 3000 | **76.31** | **1.526** | 76.53 | 1.531 | 76.44 | 1.529 | 73.75 | 1.475 |
| Mean difference | | 1.58% | | 1.40% | | 1.62% | | – |

Note: UFEM = "Unenriched" FEM = Standard ALEGRA.

Table 5 lists the actual computer run elapsed time for each simulation with the projectile velocities. The ALEGRA runs were performed using 64 nodes (512 processors) on RedSky. The X-FEM algorithm spent longer time than the standard U-FEM algorithms by a factor of 3 to 4. The *donor* algorithm spent relatively shorter time than others, with similar accuracy. (This outcome is not expected for all classes of problems.)

**Table 5: Actual elapsed time for the computer run.**

| Projectile Velocity (m/s) | X-FEM (hh:mm:ss) | UFEM, *aggressive* (hh:mm:ss) | UFEM, *donor* (hh:mm:ss) |
|---|---|---|---|
| 500 | 03:46:09 | 01:07:47 | 00:52:45 |
| 1000 | 04:49:08 | 01:28:15 | 01:04:43 |
| 1500 | 04:09:38 | 01:15:55 | 00:50:25 |
| 2000 | 04:23:05 | 01:27:55 | 01:07:45 |
| 2500 | 03:56:44 | 01:23:02 | 01:03:35 |
| 3000 | 03:39:38 | 01:21:03 | 01:00:56 |

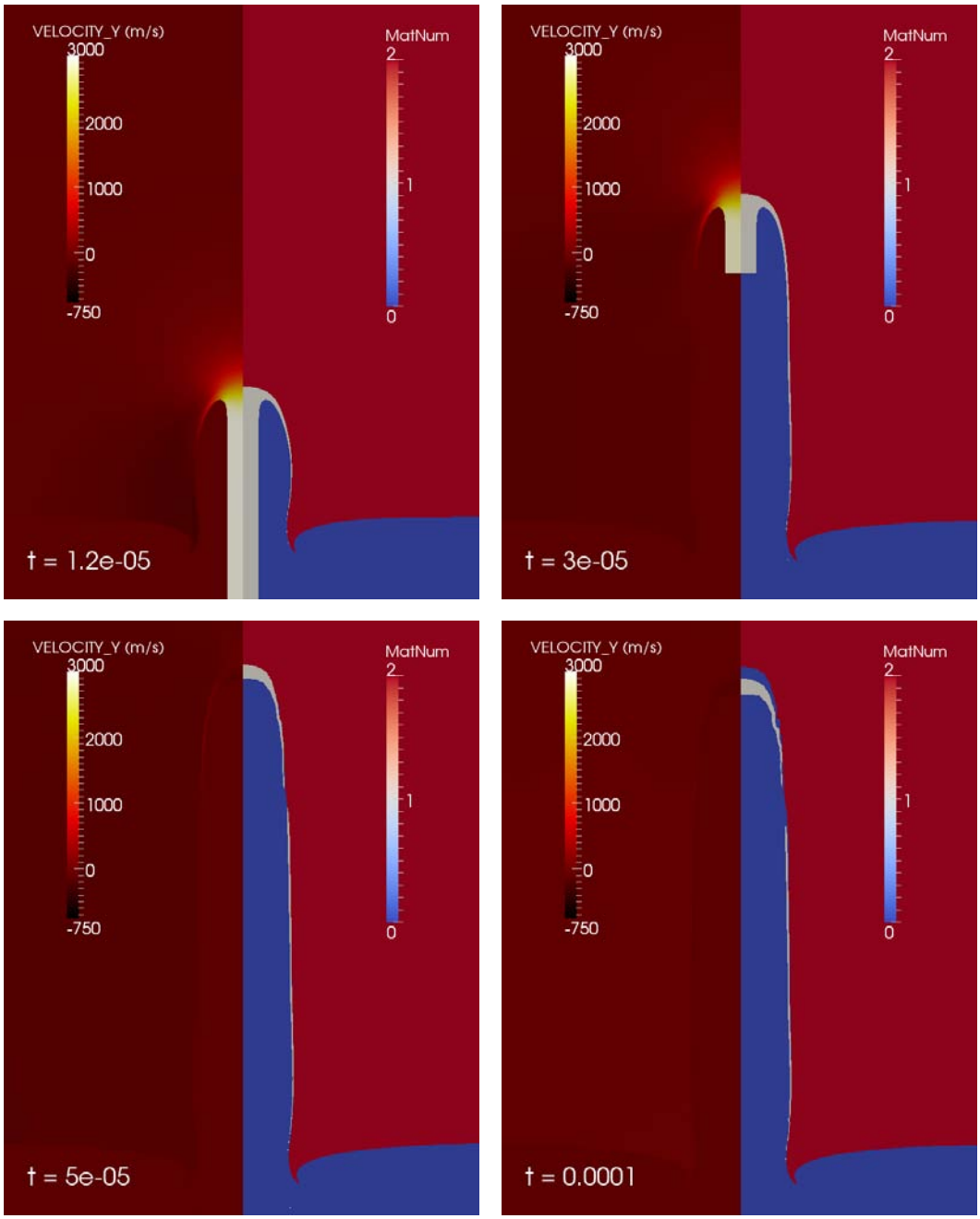


**Figure 18: Simulation results using X-FEM algorithm with projectile velocity 3000 m/s. Contours of the axial velocity are plotted on the left, and contours of the material number on the right. Simulation times are 12, 30, 50 and 100 μs.**

Figure 18 presents a series of views of the progression of the formation of the penetration channel and stagnation/recoil of the penetrator, using ALEGRA with the X-FEM algorithm for the projectile velocity of 3000 m/s. Four times are presented with the left side of each panel plotting the *z*-velocity field, and the right side showing the local material number. The input decks for the simulations are provided in Appendix 1. We observe that using X-FEM, the penetrator detaches from the end of the channel after stagnation. This recoil effect was not seen in any U-FEM simulations, which force the materials to remain joined.

## 4.4. Model boundary condition and geometry effect

To examine the model boundary condition and geometry effect, the test cases described in Table 1 and Table 6 are used for the X-FEM simulation. Figure 19 and Figure 20 show the meshes for Test cases 4x18fixed and 5x12fixed, respectively. The cell sizes of the meshes are constructed as close as possible to the baseline cell size to reduce the difference due to the cell size. The input deck for Test cases 4x18fixed and 5x12fixed are provided in Appendices 2 and 3, respectively.

**Table 6: Comparison of mesh and boundary for each test case.**

| Test case | Type | Input cell size (mm) | Cell size in penetration area (mm) | | | No. of elements | Boundary Condition | | | Figure |
|---|---|---|---|---|---|---|---|---|---|---|
| | | | $\Delta r$ | $\Delta z$ | $h$ | | Center | Edge | Back | |
| Baseline | Graded | 0.15 | 0.052 | 0.073 | 0.063 | 301644 | Fixed | Fixed | Fixed | Figure 10 |
| 4x12free | Graded | 0.15 | 0.052 | 0.073 | 0.063 | 301644 | Fixed | Fixed | Free | Figure 10 |
| 4x18fixed | Graded | 0.15 | 0.059 | 0.075 | 0.067 | 317955 | Fixed | Fixed | Fixed | Figure 19 |
| 5x12fixed | Graded | 0.15 | 0.048 | 0.083 | 0.065 | 294000 | Fixed | Fixed | Fixed | Figure 20 |

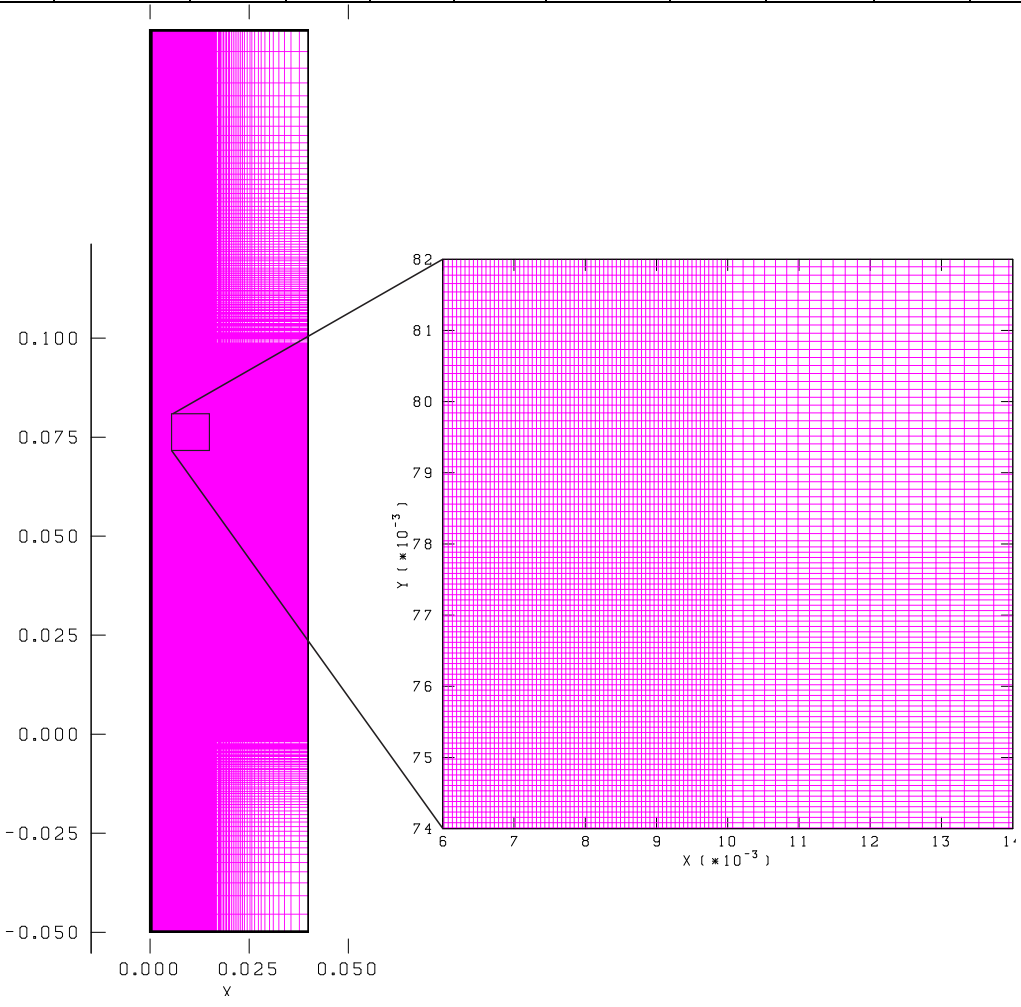


**Figure 19: Computational mesh used to examine target plate thickness (Unit on axes: m).**

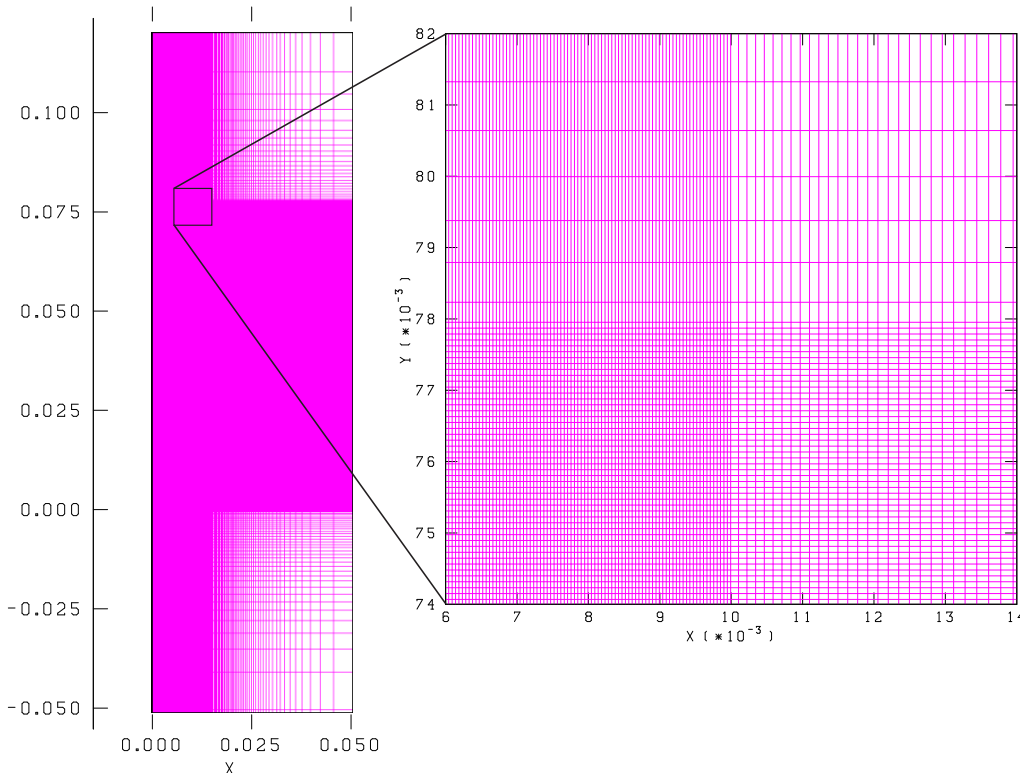


**Figure 20: Computational mesh used to examine the target plate radius. (Unit on axes: m).**

### *4.4.1. Target boundary*

To represent the semi-infinite impact/penetration scenario, no displacement boundary condition is applied on the center, right, and back of the plate in the baseline model. However, the steel target cannot be semi-infinite in the actual experimental environment, *i.e.* the thickness of target plate cannot be infinite. To represent the experimental environment, the free boundary condition can be applied on the plate back. Which boundary condition is better expression for the actual environment is studied in this section.

The normalized penetrations from the models with the plate back fixed (Baseline model) and plate back free boundary conditions are slightly different as shown Figure 21 and Table 7. Figure 22 shows the predicted DOP, rod head, and plate surface histories from the model with plate back free boundary condition. The rod head depth increases continually with time, after a brief drop just past the peak as shown Figure 15 in the baseline case. We speculate that the motion of the plate after projectile stagnation in the free-boundary case increases the DOP in a way that would not occur in a truly semi-infinite target. To represent the experimental target plate, which was effectively semi-infinite, it seems that the fixed boundary condition is appropriate. For the projectile velocity of 500 m/s, the X-FEM simulation stopped at 19.9 μs, reporting an "impossible node position" in the remap algorithm.

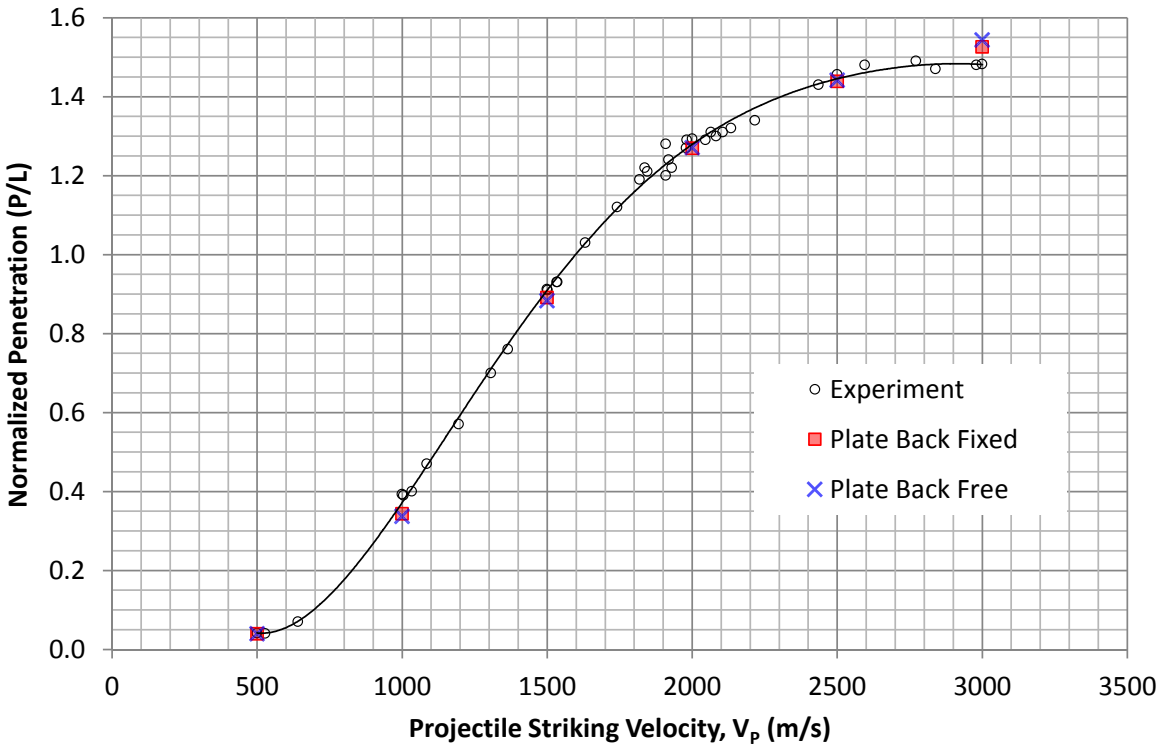


**Figure 21: Comparison of the normalized penetration depths from the models with plate back fixed (Baseline) and plate back free boundary conditions.**

**Table 7: Predicted DOP and P/L from the model with plate back fixed and free boundary conditions with polynomial-fit experimental data. (The bold fonts indicate the closer result to the experimental data).**

| Projectile Velocity (m/s) | X-FEM, Back Fixed | | X-FEM, Back Free | | Data (fit) | |
|---|---|---|---|---|---|---|
| | DOP (mm) | P/L | DOP (mm) | P/L | DOP (mm) | P/L |
| 500 | **1.98** | **0.040** | 1.97 | 0.039 | 2.07 | 0.041 |
| 1000 | **17.18** | **0.344** | 16.83 | 0.337 | 18.55 | 0.371 |
| 1500 | **44.55** | **0.891** | 44.14 | 0.883 | 45.42 | 0.908 |
| 2000 | 63.47 | 1.269 | **63.54** | **1.271** | 63.82 | 1.276 |
| 2500 | 71.95 | 1.439 | **72.09** | **1.442** | 72.06 | 1.441 |
| 3000 | **76.31** | **1.526** | 77.18 | 1.544 | 73.75 | 1.475 |

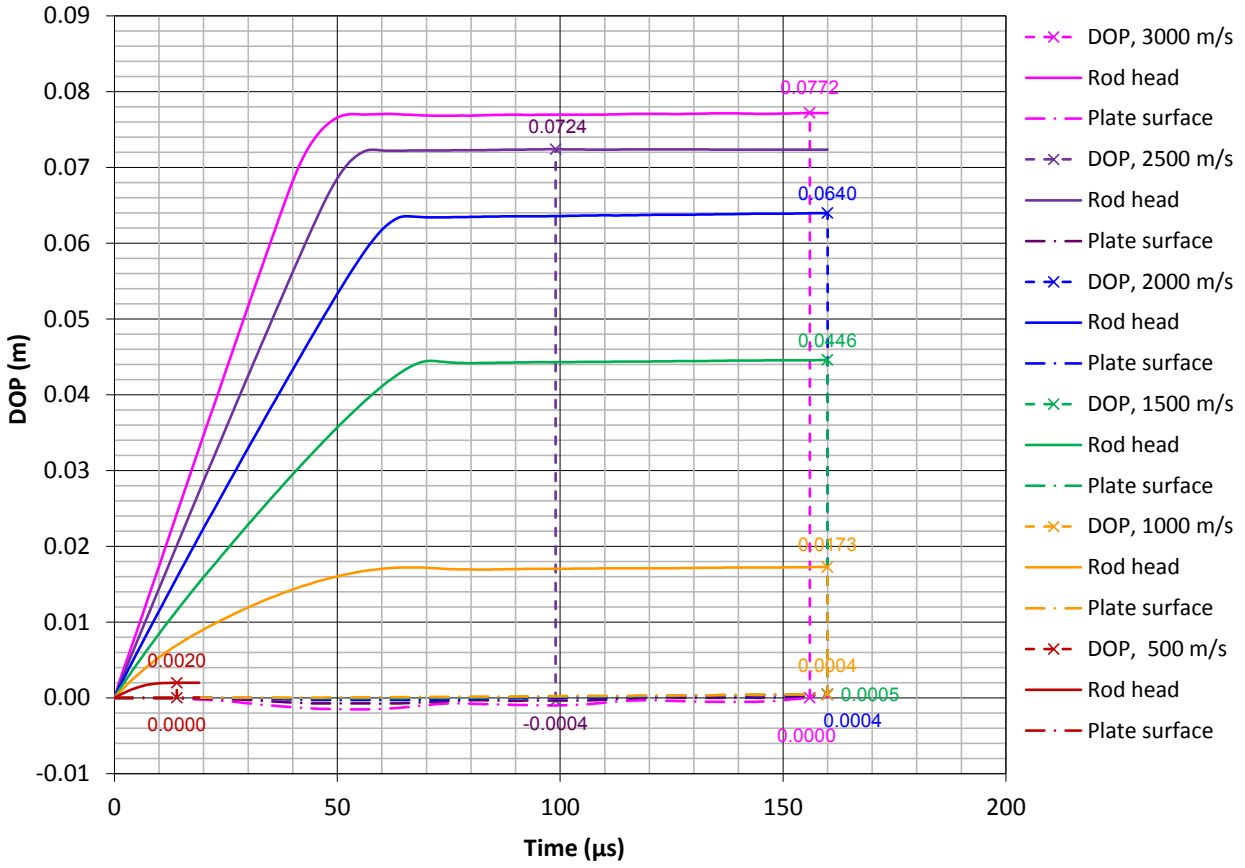


**Figure 22: Predicted DOP, rod head and plate surface histories with six velocities of rod from the model with plate back free boundary condition.**

### *4.4.2. Target plate thickness*

To investigate how the target plate thickness in the model affects the result, an X-FEM simulation is conducted with the mesh as shown in Figure 19. The target plate thickness is extended to 180 mm, and its radius is kept at 40 mm. The other conditions such as material properties and boundary conditions are the same as the baseline. The normalized penetration depths for six velocities from Test Cases 4x12fixed (baseline) and 4x18fixed are close to each other as shown Figure 23. The predicted DOP and P/L from the baseline model are slightly closer to the experimental data as listed in Table 8. In conclusion, the target plate thickness of 120 mm is enough to represent the experimental environment.

Figure 24 shows the predicted DOP, rod head, and plate surface histories from the model with the target plate thickness of 180 mm. The results are almost the same as the baseline's (Figure 15) except the depth of rod head is slightly deeper for the high velocity projectile (3000 and 2500 m/s). The X-FEM simulation stopped at 16.9 µs and 62.5 µs when the projectile velocities are 500 m/s and 1000 m/s, respectively, again reporting an "impossible node position" in the remap operation.

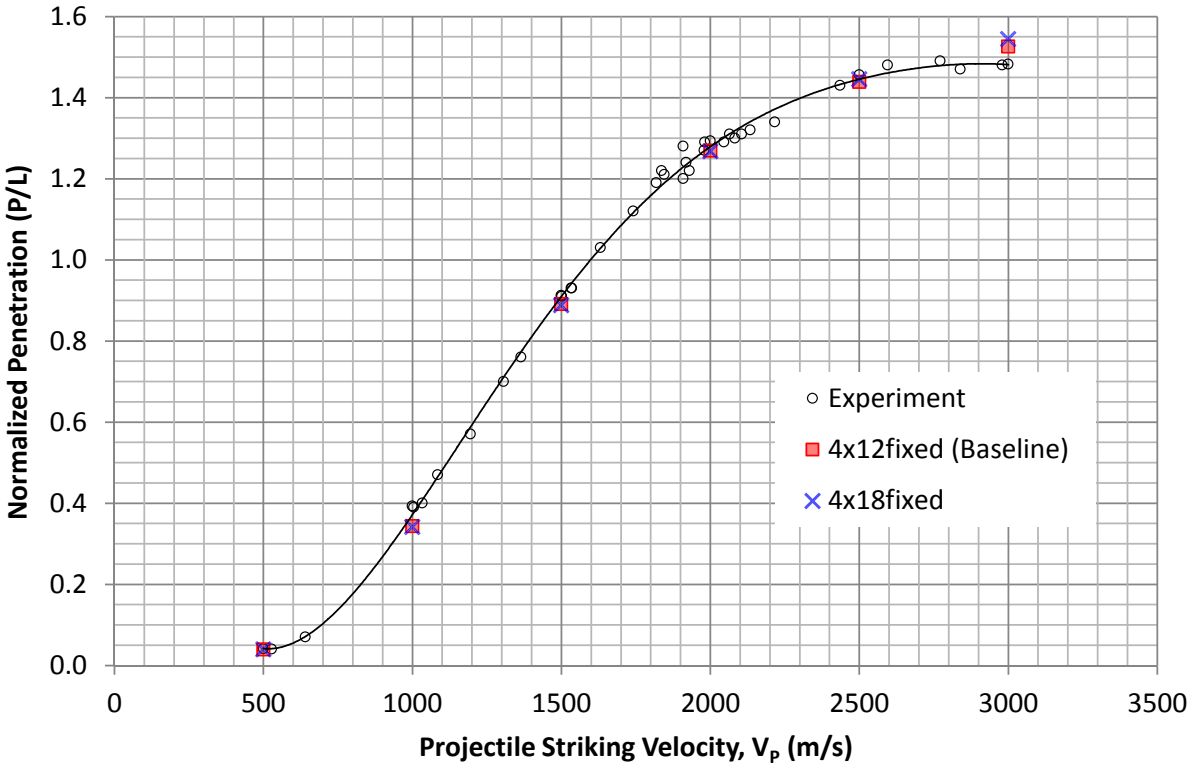


**Figure 23: Comparison of the normalized penetration depths from the models with plate thicknesses of 12 cm (Baseline) and 18 cm.**

**Table 8: Predicted DOP and P/L from the model with target plate thicknesses of 120 mm and 180 mm with polynomial-fit experimental data. (The bold fonts indicate the closer result to the experimental data).**

| Projectile Velocity (m/s) | 4x12 (Baseline) | | 4x18fixed | | Data (fit) | |
|---|---|---|---|---|---|---|
| | DOP (mm) | P/L | DOP (mm) | P/L | DOP (mm) | P/L |
| 500 | **1.98** | **0.040** | 1.96 | 0.039 | 2.07 | 0.041 |
| 1000 | **17.18** | **0.344** | 17.07 | 0.341 | 18.55 | 0.371 |
| 1500 | **44.55** | **0.891** | 44.40 | 0.888 | 45.42 | 0.908 |
| 2000 | **63.47** | **1.269** | 63.39 | 1.268 | 63.82 | 1.276 |
| 2500 | 71.95 | 1.439 | **72.28** | **1.446** | 72.06 | 1.441 |
| 3000 | **76.31** | **1.526** | 77.21 | 1.544 | 73.75 | 1.475 |

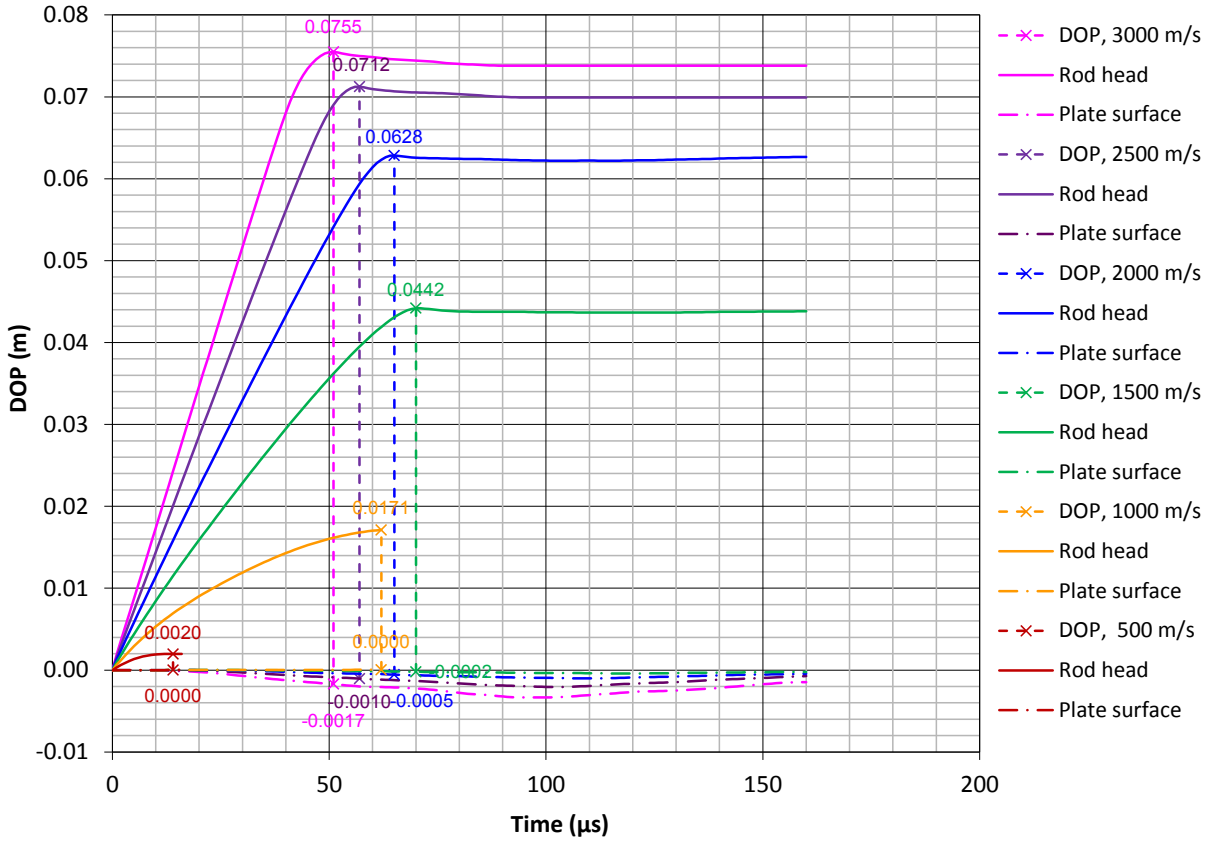


**Figure 24: Predicted DOP, rod head and plate surface histories with six velocities of rod from the model with target plate thickness of 180 mm.**

### *4.4.3. Target plate radius*

To investigate how the target plate radius in the model affects the result, an X-FEM simulation is conducted with the mesh as shown in Figure 20 (Target plate thickness is 120 mm, radius is 50 mm). The other conditions such as material properties, boundary conditions, etc. are the same as the baseline. The normalized penetration depths for six velocities from Test Case 4x12fixed (baseline) and 5x12fixed are close each other as shown Figure 25 and Table 9. In conclusion, the target plate radius of 40 mm is enough to represent the experimental environment.

Figure 26 shows the predicted DOP, rod head, and plate surface histories from the model with the target plate radius of 50 mm. The results are almost the same as the baseline's (Figure 15). The X-FEM simulation stopped at 27.7 µs and 65.6 µs when the projectile velocities are 500 m/s and 1000 m/s, respectively. The error messages reported "impossible node position" in remap for the 500-m/s case, and "significant overfill" in the 1000-m/s case.

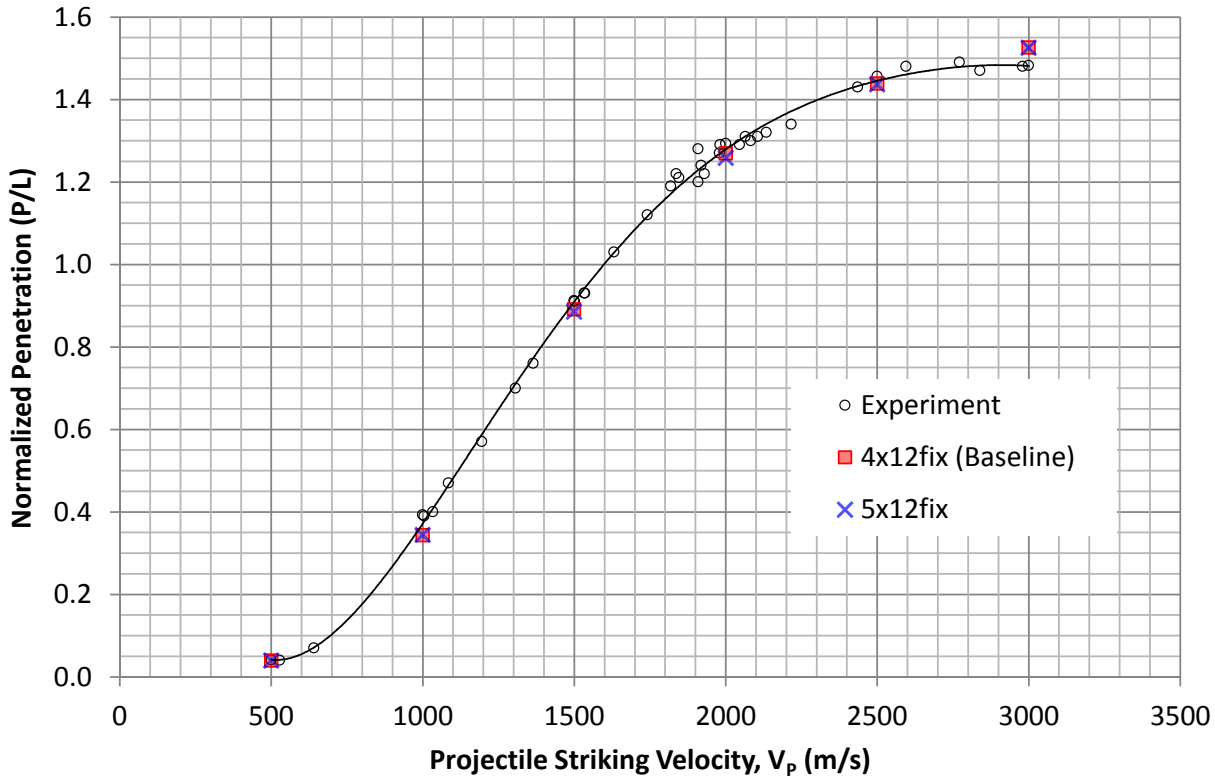


**Figure 25: Comparison of the normalized penetration depths from the models with plate radius of 40 mm (Baseline) and 50 mm.**

**Table 9: Predicted DOP and P/L from the model with target plate radius of 40 mm and 50 mm with experimental data. (The bold fonts indicate the closer result to the experimental data).**

| Projectile Velocity (m/s) | 4x12fixed (Baseline) | | 5x12fixed | | Experimental Data | |
|---|---|---|---|---|---|---|
| | DOP (mm) | P/L | DOP (mm) | P/L | DOP (mm) | P/L |
| 500 | 1.98 | 0.040 | **1.99** | **0.040** | 2.05 | 0.041 |
| 1000 | 17.18 | 0.344 | **17.20** | **0.344** | 19.68 | 0.393 |
| 1500 | **44.55** | **0.891** | 44.27 | 0.885 | 45.67 | 0.912 |
| 2000 | **63.47** | **1.269** | 62.93 | 1.259 | 64.75 | 1.293 |
| 2500 | **71.95** | **1.439** | 71.83 | 1.437 | 72.91 | 1.456 |
| 3000 | 76.31 | 1.526 | **76.27** | **1.525** | 74.21 | 1.482 |

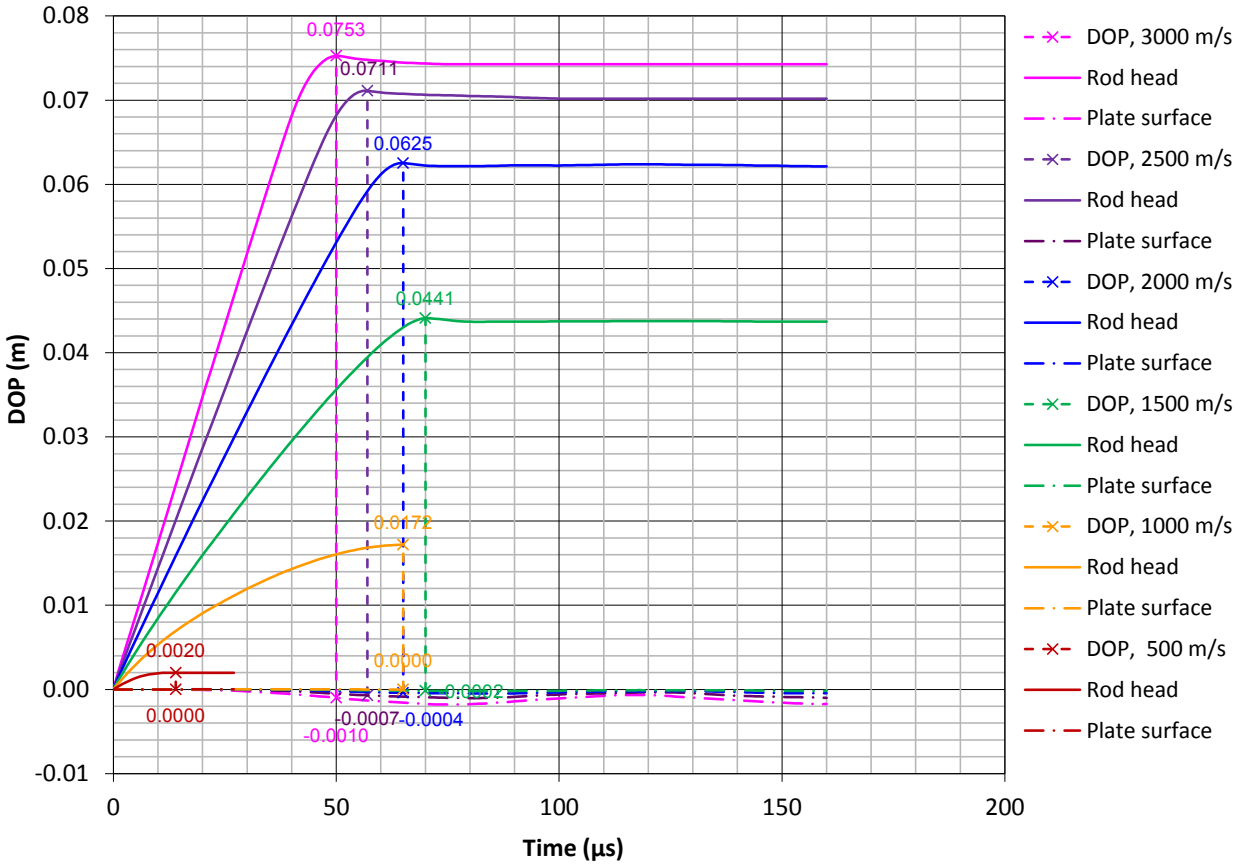


**Figure 26: Predicted DOP, rod head and plate surface histories with six velocities of rod from the model with target plate radius of 50 mm.**

## 5. SUMMARY AND CONCLUSIONS

The simulations conducted in this study provide the first evaluation of the X-FEM implementation in ALEGRA for classical problems in high-velocity impact and penetration. The results demonstrate that the new algorithm reproduces the excellent results obtained using the standard algorithms in ALEGRA, and retains their accuracy. Depths of penetration computed using X-FEM over the impact velocity range 500 m/s $\leq V_P \leq$ 3000 m/s differ from the experimental data of Hohler and Stilp (1977,1987) [8,9] by only 1.6%. They differ from the standard-formulation results with high-order remap by only 0.5%. They also provide improved depth of penetration compared to the standard-formulation results with low-order remap (see Table 4 and Figures 17 and 18).

The various sensitivities of the computed X-FEM solutions have been examined here. The solution converges at a rate that is consistent with the expected behavior for solutions containing shocks: the depth of penetration converges smoothly and monotonically at first order

(convergence rate $1.057 \leq c \leq 1.066$, see Figure 14). Sensitivities to domain size and boundary conditions for this particular problem have also been examined to ensure correct setup of the problem. Sensitivity to these parameters is relatively weak, so that the baseline configuration used here is shown to be adequate (see Tables 7-9 and associated figures).

The results here show that the performance cost of the upgrade from standard methods to X-FEM is a factor of 3 to 4 in compute time for this class of problems (see Table 5). The implementation has been tested for parallel scaling with good results. However, no concerted attempt has been made to optimize the X-FEM code for speed and efficient memory use. This is slated for work in the near future, and we therefore expect improved performance to be observed soon. We also note that out of 29 total X-FEM simulations conducted in the present study, 5 stopped before completion with errors, as described in Section 4. The robustness of the implementation is expected to improve as current active development efforts proceed. A 3D extension of the X-FEM capability is also in progress, and we anticipate testing of the 3D capability using the Hohler-Stilp data in future work as well.

The ballistic environment considered here is dominated by hydrodynamic interaction of the penetrator and target materials. The present results show that the X-FEM reproduces the accuracy of the standard Eulerian method in ALEGRA that has already been established for this class of problems. The high quality of the results produced using ALEGRA with X-FEM for these cases suggests that this software is ready for production use, and for testing in other situations where the accuracy of the standard Eulerian method has not been well established.

# 6. REFERENCES


1 Anderson, Jr., C. E., Hohler, V., Walker, J. D. and Stilp, A. J., 1995. Time-resolved penetration of long rods into steel targets, *Int. J. Impact. Engng.* Vol 16, No 1, pp. 1-18.

2 Anderson, Jr., C. E., Morris, B. L. and Littlefield, D. L., 1992. *A Penetration Mechanics Database*, Southwest Research Institute Report 3593/001, San Antonio, TX, January.

3 Anderson, Jr., C. E. and Walker, J. D., 1991. An examination of long-rod penetration, *Int. J. Impact Engng.* Vol 11, No. 4, pp. 481-501.

4 Blanks, J. R., 1983. *Ballistic Research Lab KE Penetrator Impact Test*, September 1983. Private communication to Paul Yarrington, Org. 9232, Sandia National Laboratory.

5 Carroll, D.E., Hertel, Jr., E.S., and Trucano, T.G., 1997. *Simulation of Armor Penetration by Tungsten Rods: ALEGRA Validation Report*, SAND97-2765, Sandia National Laboratories, Albuquerque, NM.

6 Dolbow, J., Mosso, S., Robbins, J., and Voth, T, 2008. Coupling volume-of-fluid based interface reconstructions with the extended finite element method, *Computer Methods in Applied Mechanics and Engineering*, Vol. 197, pp. 439-447.

7 Doney, R. L., Vunni, G. B., and Niederhaus, J. H, 2010. *Experiments and simulations of exploding aluminum wires: validation of ALEGRA-MHD*, U.S. Army Research Laboratory technical report ARL-TR-5299, Aberdeen Proving Ground, MD, September.

8 Hohler, V. and Stilp, A.J., 1977. Penetration of steel and high density rods in semi-infinite steel targets, *Proceedings of the 3rd International Symposium on Ballistics*, Karlsruhe, Germany, March.

9 Hohler, V. and Stilp, A.J., 1987. Hypervelocity Impact of Rod Projectiles with L/D from 1 to 32, *International Journal Impact Engineering*, Vol. 5, pp. 323-331, 1987, Printed in Great Britain.

10 Johnson, G.R. and Cook, W.H., 1993. A Constitutive Model and Data for Metals Subjected to Large Strains, High Strain Rates and High Temperatures, in *Proceedings of Seventh International Symposium on Ballistics.* The Hague. The Netherlands, April.

11 Kamm, J. R., Rider, W. J., Witkowski, W. R., Trucano, T. G., and Ben-Haim, Y., 2012. Info-gap analysis of the numerical uncertainty associated with truncation error in discretized solution of differential equations, Manuscript in preparation.

12 Kmetyk, L. N. and Yarrington, P., 1988. *Cavity Dimensions for High Velocity Penetration Events – a Comparison of Calculational Results with Data*," SAND88-2693, Albuquerque, NM.

13 Lanz, W. and Odermatt, W., 1992. Penetration limits of conventional large caliber anti tank guns / kinetic energy projectiles, in *Proceedings of the 13th International Symposium on Ballistics*, Stockholm, Sweden, June.

14 Lemke, R. W., Knudson, M. D., Bliss, D. E., Cochrane, K., Davis, J.-P., Giunta, A. A., Harjes, H. C., and Slutz, S. A., 2005. Magnetically accelerated, ultrahigh velocity flyer plates for shock wave experiments, *Journal of Applied Physics*, Vol. 98, 073530.

15 Rapacki, Jr., E. J., Frank, K., Leavy, R. B., Keele, M. J., Prifti, J. J. 1995. Armor Steel Hardness Influence on Kinetic Energy Penetration, in *Proceedings of the 15th International Symposium on Ballistics*, Jerusalem, Israel, May.

16 Rider, W. J. and Kamm, J. R., 2012. Advanced solution verification of CFD solutions for LES of relevance to GTRF estimates, SAND2012-7199P, Sandia National Laboratories, Albuquerque, NM.

17 Rider, W. J., Love, E., Wong, M. K., Strack, O. E., Petney, S. V., and Labreche, D. A., 2011. Adaptive methods for multi-material ALE hydrodynamics, *International Journal for Numerical Methods in Fluids*, Vol. 65, pp. 1325-1337.

18 Robinson, A. C., Rider, W. J., et al., 2008. ALEGRA: An Arbitrary Lagrangian-Eulerian Multimaterial, Multiphysics Code. *In Proceedings of the 46th AIAA Aerospace Sciences Meeting*, Reno, NV, AIAA 2008-1235.

19 Sharp. G, Niederhaus, J. H. J., Voth, T., Mosso, S., and Park, B.-Y., 2012. Modeling of high-velocity impacts on finit-thickness and semi-infinite targets using XFEM in ALEGRA, 2012 Research in Ballistic Protection Technologies. Aberdeen Proving Grounds, MD, May.

20 Subramanian, R. and Bless, S. J. 2001. Reference correlations for tungsten long rods striking semi-infinite steel targets, in *Proceedings of the 19th International Symposium on Ballistics*, Interlaken, Switzerland, May.

21 Templeton, D., Holmquist, T., Meyer, H., Grove, D., and Leavy, B., 2002. A Comparison of Ceramic Material Models, *Ceramic Armor Materials by Design*, Vol. 134.

22 Voth, T., Mosso, S., Niederhaus, J., and Kipp, M., 2011. An implementation of the X-FEM for Eulerian solid-mechanics, *11$^{th}$ U.S. National Congress on Computational Mechanics*. Minneapolis, MN, July.

23 Voth, T. and Mosso, S., 2012. An eXtended finite element/Eulerian (XFEM/Eulerian) approach for solid mechanics, 2012 Research in Ballistic Protection Technologies. Aberdeen Proving Grounds, MD, May.

# APPENDIX: INPUT DECK

[units.txt]

```
$Unit conversion (A_B = A to B):
$
$Angular:
$ rad  = {rad_deg  =180/3.1415926536} deg
$ deg  = {deg_rad  =1/rad_deg} rad
$
$Length:
$ mm   = {mm_m=0.001 } m
$ m    = {m_mm=1/mm_m} mm
$ cm   = {cm_mm=10 } mm
$ mm   = {mm_cm=1/cm_mm} cm
$ cm   = {cm_m=0.01  } m
$ m    = {m_cm=1/cm_m} cm
$ ft   = {ft_m=0.3048} m
$ m    = {m_ft=1/ft_m} ft
$ in   = {in_m=0.0254} m
$ m    = {m_in=1/in_m} in
$
$Pressure:
$ MPa  = {MPa_Pa  = 1E6} Pa
$ Pa   = {Pa_MPa  = 1/MPa_Pa} MPa
$ psi  = {psi_Pa=6894.757} Pa
$ Pa   = {Pa_psi=1/psi_Pa} psi
$ Pa   = {Pa_psf=0.0208854} psf
$ psf  = {psf_Pa=1/Pa_psf} Pa
$ MPa  = {MPa_psf=MPa_Pa*Pa_psf} psf
$ MPa  = {MPa_psi=MPa_Pa*Pa_psi} psi
$ psf  = {psf_psi=psf_Pa*Pa_psi} psi
$
$Time:
$ mus  = {mus_s   = 1e-6         } s
$ min  = {min_s   = 60           } s
$ h    = {h_min   = 60           } min
$ d    = {d_h     = 24           } h
$ mon  = {mon_d   = 30.4166666667} d
$ yr   = {yr_d    = 365          } d
$ dec  = {dec_yr  = 10           } yr
$ cen  = {cen_dec = 10           } dec
$ mil  = {mil_cen = 10           } cen
$ h    = {h_s     = h_min*min_s  } s
$ d    = {d_s     = d_h*h_s      } s
$ mon  = {mon_s   = mon_d*d_s    } s
$ yr   = {yr_s    = yr_d*d_s     } s
$ dec  = {dec_s   = dec_yr*yr_s  } s
$ cen  = {cen_s   = cen_dec*dec_s} s
$ mil  = {mil_s   = mil_cen*cen_s} s
$ s    = {s_mus   = 1/mus_s      } mus
$ s    = {s_min   = 1/min_s      } min
$ s    = {s_h     = 1/h_s        } h
$ s    = {s_mon   = 1/mon_s      } mon
$ s    = {s_yr    = 1/yr_s       } yr
```

## Appendix 1: Input deck for 4x12fixed

[parameters.txt]

```
$
$ Define Parameters
$
$ Test Case:                     T_CAS = {T_CAS='subM'}
$ Cell size:                     S_CEL = {S_CEL=0.15*mm_m} m
$ Model Center (X):              C_MDL = {C_MDL=  0.00} m
$ Radius of Plate (X):           R_PLT = {R_PLT= 40.0*mm_m} m
$ Thickness of Plate (Y):        T_PLT = {T_PLT= 120.0*mm_m} m
$ Radius of Rod (X):             R_ROD = {R_ROD= 2.5*mm_m} m
$ Length of Rod (Y):             L_ROD = {L_ROD= 50.0*mm_m} m
$ Velocity of Rod:               V_ROD = {V_ROD= 500} m/s
$ Front of Plate (Y):            F_PLT = {F_PLT= 0.00} m
$ Back of Plate (Y):             B_PLT = {B_PLT= F_PLT+T_PLT} m
$ Head of Rod (Y):               H_ROD = {H_ROD= F_PLT} m
$ Tail of Rod (Y):               T_ROD = {T_ROD= H_ROD-L_ROD} m
$ Back of Model (Y):             B_MDL = {B_MDL= R_PLT} m
$ Front of 1st Graded Area (Y):  F_1GA = {F_1GA= 78.*mm_m} m (hole depth is 0.0741 at 3000 m/s)
```

```
$ Radius of 1st Graded Area (X): R_1GA = {R_1GA= 4.*R_ROD} m
$ Gap between Rod tail and Front of Model (Y): L_GAP = {L_GAP= S_CEL} m
$ Front of Model (Y):            F_MDL = {F_MDL= T_ROD-L_GAP} m
$ Length of Model (Y):           L_MDL = {L_MDL= T_PLT+L_ROD+L_GAP} m
```

Note: V_ROD varied from 500 m/s to 3000 m/s for the projectile rod velocities.

[hohlerstilprha.inp] for subcase 5-G

```
$ {include("/home/bypark/common/units.txt")}
$ {_FORMAT="%.10g"}
$ --- COMMENTS ---
$     Author:          Brian Leavy
$     Modified:                Byoung Yoon Park 12-02-2011
$     Experiment:      Hohler & Stilp W rod vs RHA
$     Comments:                Validation test for X-FEM in ALEGRA

$=== VARIABLES====
$ {include("parameters.txt")}
$ Time Interval:    {T_INT = 1.0e-6} s
$ Plot Interval:    {P_INT = T_INT} s

$ === EXECUTION CONTROL ===
$ --- Initiation and Termination
Title
Hohler-Stilprha {T_CAS}, v={V_ROD} m/s, R={R_ROD*m_mm} mm, L={L_ROD*m_cm} cm, CELL={S_CEL*m_mm}
mm

units, si
READ RESTART DUMP = -1        $ Restart at the latest available restart dump
termination time, {tt=160.0e-6}       $ Simulation terminated at {tt*s_mus} mus.
TERMINATION CPU {tc=6.*h_s}   $ Run will be terminated within CPU time 1hr/64nodes(Agg)
$termination cycle, 1
CHECK SHUTDOWN FILE {csf=2}m          $ Check shutdown file every {csf} minutes
EMIT RESTART, TIME INTERVAL {T_INT} $ Make dmp file every {T_INT*s_mus} mus.

$--- I/O Control
emit plot, time interval={P_INT} $ s
$emit plot, cycle interval=10 from time 7.e-5 to 15.e-5
emit hisplt, cycle interval=10
$emit hisplt, time interval={T_INT} $ s
$emit hisplt, cycle interval=1 from time 7.e-5 to 15.e-5

plot variables
  no_underscores
  velocity
  density
  density,avg
  temperature
  temperature,avg
  pressure
  pressure,avg
  mat_min_coords
  mat_max_coords
end

history plot variables
  no_underscores
  velocity
  density
  temperature
  pressure
end

spy

  PlotTime(0.0,{P_INT});

  define main()
  \{
    pprintf(" PLOT: Cycle=%d, Time=%e\n",CYCLE,TIME);
    % ListVariables();

    Image("HohlerStilpRha",WHITE,BLACK);
      Label("{T_CAS}, v={V_ROD} m/s, Graded cell={S_CEL*m_mm} mm");
      SMOOTH_SHADING = OFF;
      ColorMapRange(0.,20000.,LIN_MAP);
      % AutoScaleMap("DENSITY",0.,20000.);
      DrawColorMap("DENSITY",0.1,0.3,0.3,0.8);
```

```
      Plot2D("DENSITY");
      Color(PURPLE);
      Draw2DMatContour;

      Color(BLACK);
      DrawText(sprintf("t = %.2f ~m~s",1.e6*TIME),0.4,0.05);
      Color(BLACK);

      LogoShading(ON);
      LogoText(ON);
      LogoColors(BLACK,CYAN,BLACK);

      LogoPosition(0.0,0.0,0.4,0.15);
      DrawSNL_Logo(1.3);
    EndImage;
  \}
endspy

$ === PHYSICS INPUT===
solid dynamics
  cylindrical
  constant volume fraction algorithm
  end

  xfem
    tangential search tolerance, 0.05
    maxenf iterations, 100
    gap rate tolerance, 1.e-8
    mspair 2,1
  end

  domain
    remap method, intersection
    pattern reconstruction
    interface order 2 0 1
    pattern smoothing = off
    pattern fragment motion = off
  end

  time step scale, {tss=.4}  $ {tss} times of the value of the calculated stable time step.

$ --- MESH ---
$BX :{BX = 1} $ Number of Blocks in X
$BY :{BY = 1} $ Number of Blocks in Y
$NX_TOT :{NX_TOT = int((R_PLT/S_CEL)/BX)}
$NY_TOT :{NY_TOT = int((L_MDL/S_CEL)/BY)}
$NX :{NX = NX_TOT/BX}
$NY :{NY = NY_TOT/BY}
$NSLOTS :{NSLOTS = BX*BY}
$NUM_CELLS :{NUM_CELLS = NX_TOT*NY_TOT}
$R_DER :{R_DER = 4.*R_ROD} $ Dense element radius bound (R-dir)
$Z_DEU :{Z_DEU = 0.078}    $ Dense element upper bound (Z-dir) (hole depth is 0.0741 at 3000 m/s)
$Z_DEL :{Z_DEL = 0.000}    $ Dense element lower bound (Z-dir)
$F_DER :{F_DER = 0.1}      $ Increase Rate (R-dir), The larger, the smaller interval
$F_DER :{F_DEU = 0.7}      $ Increase Factor (+Z-dir), The larger, the smaller interval
$F_DEL :{F_DEL = 0.3}      $ Increase Factor (-Z-dir), The larger, the larger interval
mesh, inline
  rectilinear
    bx = {BX}
    by = {BY}
    nx = {NX}
    ny = {NY}
    gmin = {C_MDL} {F_MDL}
    gmax = {NX_TOT*BX*S_CEL}  {F_MDL+NY_TOT*BY*S_CEL}
  end
  set assign
    sideset,ilo,30
    sideset,ihi,10
    sideset,jlo,40
    sideset,jhi,20
  end
  USER DEFINED ELEMENT DENSITY, X
    "
      field=1;
      if(coord <  {R_DER}) {"{"}field = 1;{"}"}
      if(coord >= {R_DER}) {"{"}field = 1.*exp(-100.*((coord)-{R_DER*F_DER}));{"}"}
    "
  END
  USER DEFINED ELEMENT DENSITY, Y
    "
      field=1;
```

```
      if(coord <  {Z_DEU}) {"{"}field = 1;{"}"}
      if(coord >= {Z_DEU}) {"{"}field = 1.*exp(-80.*((coord)-{Z_DEU*F_DEU}));{"}"}
      if(coord <= {Z_DEL}) {"{"}field = 1.*exp( 70.*((coord)-{Z_DEU*F_DEL}));{"}"}
      if(coord <  {T_ROD}) {"{"}field = 1;{"}"}
    "
  END
end
$$
$ --- BOUNDARY CONDITION ---
  no displacement, sideset 20,z $ +Z
  no displacement, sideset 10,r $ +R
  no displacement, sideset 30,r $ -R = 0

  block 1
    EULERIAN MESH
    add diatom input
  end

$ --- MATERIAL INSERTION ---
$----------------------------------------
$  material 1, rod, 93% WHA, Tungsten
$  material 2, plate, HzB Steel
$----------------------------------------
  diatom
    translate(0.,{H_ROD})
     package 'ROD'
       material 1
       yvelocity {V_ROD}
       insert box
         p1      {C_MDL} {H_ROD}
         p2      {R_ROD} {T_ROD}
       endi
     endp
    endt
    translate(0.,{F_PLT})
     package 'PLATE'
       material 2
       insert box
         p1      {C_MDL} {F_PLT}
         p2      {R_PLT} {B_PLT}
       endi
     endp
    endt
  enddiatom

$ --- TRACERS ---
  tracer points
    lagrangian Tracer 1  x  {C_MDL}        y {H_ROD}   $ Center of Rod Head  -- Tracer H
    lagrangian tracer 2  x  {C_MDL}        y {T_ROD}   $ Center of Rod Tail
    lagrangian tracer 3  x  {C_MDL}        y {F_PLT}   $ Center of Plate Front
    lagrangian tracer 4  x  {R_PLT-S_CEL}  y {F_PLT}   $ Edge of Plate Front -- Tracer P
    lagrangian tracer 5  x  {R_ROD}        y {F_PLT}   $ Edge of Rod on Plate Front
  end

  plot, exotracer
    file = 'tracer.exo'
  end

$ plot, vtk mesh
$   file = 'hohlerstilprha'
$ end

end

$ === MATERIAL ===
material 1              $ 93% WHA
  model = 1
end
model 1 cth elastic plastic
  eos model      = 100
  yield model    = 10
$  fracture model = 1000
end
model 10 johnson cook ep
  ajo = 1.365e9         $ Hohler & Stilp
  bjo = 0.1765e9
  cjo = 0.016
  mjo = 1.00
  njo = 0.12
  tjo = 3695.
  poisson = 0.281
```

```
end
model 100, keos sesame
  feos = 'sesame'
  neos = 3550            $ TUNGSTEN
  sr   = 1.094           $ Scaled for 17.760 g/cc
  clip = 1.0
end

material 2               $ HzB Steel
  model = 2
end
model 2 cth elastic plastic
  eos model      = 200
  yield model    = 20
end
model 20 johnson cook ep
  ajo=0.810e9            $ Hohler & Stilp HzB
  bjo=0.5095e9
  cjo=0.014
  mjo=1.030
  njo=0.260
  tjo=1818.
  poisson = 0.299
end
model 200, keos sesame
  feos = 'sesame'
  neos = 2150            $ Iron
  sr   = 1.003           $ Scaled for 7.85 g/cc
  clip = 1.0
end

exit
```

[hohlerstilprha.inp] for U-FEM *aggressive* remap simulation

```
$ {include("/home/bypark/common/units.txt")}
$ {_FORMAT="%.10g"}
$ --- COMMENTS ---
$     Author:          Brian Leavy
$     Modified:                Byoung Yoon Park 12-02-2011
$     Experiment:      Hohler & Stilp W rod vs RHA
$     Comments:                Validation test for X-FEM in ALEGRA

$=== VARIABLES====
$ {include("parameters.txt")}
$ Time Interval:    {T_INT = 1.0e-6} s
$ Plot Interval:    {P_INT = T_INT} s

$ === EXECUTION CONTROL ===
$ --- Initiation and Termination
Title
Hohler-Stilprha {T_CAS}, v={V_ROD} m/s, R={R_ROD*m_mm} mm, L={L_ROD*m_cm} cm, CELL={S_CEL*m_mm}
mm

units, si
READ RESTART DUMP = -1        $ Restart at the latest available restart dump
termination time, {tt=160.0e-6}       $ Simulation terminated at {tt*s_mus} mus.
TERMINATION CPU {tc=6.*h_s}   $ Run will be terminated within CPU time 1hr/64nodes(Agg)
$termination cycle, 1
CHECK SHUTDOWN FILE {csf=2}m          $ Check shutdown file every {csf} minutes
EMIT RESTART, TIME INTERVAL {T_INT} $ Make dmp file every {T_INT*s_mus} mus.

$--- I/O Control
emit plot, time interval={P_INT} $ s
emit hisplt, cycle interval=10

plot variables
  no underscores
  velocity
  density
  density,avg
  temperature
  temperature,avg
  pressure
  pressure,avg
  mat_min_coords
  mat_max_coords
end
```

```
history plot variables
  no_underscores
  velocity
  density
  temperature
  pressure
end

spy

  PlotTime(0.0,{P_INT});

  define main()
  \{
    pprintf(" PLOT: Cycle=%d, Time=%e\n",CYCLE,TIME);
    % ListVariables();

    Image("HohlerStilpRha",WHITE,BLACK);
      Label("{T_CAS}, v={V_ROD} m/s, Graded cell={S_CEL*m_mm} mm");
      SMOOTH_SHADING = OFF;
      ColorMapRange(0.,20000.,LIN_MAP);
      % AutoScaleMap("DENSITY",0.,20000.);
      DrawColorMap("DENSITY",0.1,0.3,0.3,0.8);
      Plot2D("DENSITY");
      Color(PURPLE);
      Draw2DMatContour;

      Color(BLACK);
      DrawText(sprintf("t = %.2f ~m~s",1.e6*TIME),0.4,0.05);
      Color(BLACK);

      LogoShading(ON);
      LogoText(ON);
      LogoColors(BLACK,CYAN,BLACK);

      LogoPosition(0.0,0.0,0.4,0.15);
      DrawSNL_Logo(1.3);
    EndImage;
  \}
endspy

$ === PHYSICS INPUT===
solid dynamics
  cylindrical
  constant volume fraction algorithm
  end

  domain
    pattern reconstruction
    interface order 2 0 1
    pattern smoothing = off
    pattern fragment motion = off
  end

  time step scale, {tss=.4}  $ {tss} times of the value of the calculated stable time step.

$ --- MESH ---
$BX :{BX = 1} $ Number of Blocks in X
$BY :{BY = 1} $ Number of Blocks in Y
$NX_TOT :{NX_TOT = int((R_PLT/S_CEL)/BX)}
$NY_TOT :{NY_TOT = int((L_MDL/S_CEL)/BY)}
$NX :{NX = NX_TOT/BX}
$NY :{NY = NY_TOT/BY}
$NSLOTS :{NSLOTS = BX*BY}
$NUM_CELLS :{NUM_CELLS = NX_TOT*NY_TOT}
$R_DER :{R_DER = 4.*R_ROD} $ Dense element radius bound (R-dir)
$Z_DEU :{Z_DEU = 0.078}    $ Dense element upper bound (Z-dir) (hole depth is 0.0741 at 3000 m/s)
$Z_DEL :{Z_DEL = 0.000}    $ Dense element lower bound (Z-dir)
$F_DER :{F_DER = 0.1}      $ Increase Rate (R-dir), The larger, the smaller interval
$F_DER :{F_DEU = 0.7}      $ Increase Factor (+Z-dir), The larger, the smaller interval
$F_DEL :{F_DEL = 0.3}      $ Increase Factor (-Z-dir), The larger, the larger interval
mesh, inline
  rectilinear
    bx = {BX}
    by = {BY}
    nx = {NX}
    ny = {NY}
    gmin = {C_MDL} {F_MDL}
    gmax = {NX_TOT*BX*S_CEL}  {F_MDL+NY_TOT*BY*S_CEL}
  end
```

```
  set assign
    sideset,ilo,30
    sideset,ihi,10
    sideset,jlo,40
    sideset,jhi,20
  end
  USER DEFINED ELEMENT DENSITY, X
    "
      field=1;
      if(coord <  {R_DER}) {"{"}field = 1;{"}"}
      if(coord >= {R_DER}) {"{"}field = 1.*exp(-100.*((coord)-{R_DER*F_DER}));{"}"}
    "
  END
  USER DEFINED ELEMENT DENSITY, Y
    "
      field=1;
      if(coord <  {Z_DEU}) {"{"}field = 1;{"}"}
      if(coord >= {Z_DEU}) {"{"}field = 1.*exp(-80.*((coord)-{Z_DEU*F_DEU}));{"}"}
      if(coord <= {Z_DEL}) {"{"}field = 1.*exp( 70.*((coord)-{Z_DEU*F_DEL}));{"}"}
      if(coord <  {T_ROD}) {"{"}field = 1;{"}"}
    "
  END
end
$$
$ --- BOUNDARY CONDITION ---
  no displacement, sideset 20,z $ +Z
  no displacement, sideset 10,r $ +R
  no displacement, sideset 30,r $ -R = 0

  block 1
    EULERIAN MESH
    add diatom input
    AGGRESSIVE ADVECTION
  end

$ --- MATERIAL INSERTION ---
$----------------------------------------
$  material 1, rod, 93% WHA, Tungsten
$  material 2, plate, HzB Steel
$----------------------------------------
  diatom
    translate(0.,{H_ROD})
     package 'ROD'
       material 1
       yvelocity {V_ROD}
       insert box
         p1      {C_MDL} {H_ROD}
         p2      {R_ROD} {T_ROD}
       endi
     endp
    endt
    translate(0.,{F_PLT})
     package 'PLATE'
       material 2
       insert box
         p1      {C_MDL} {F_PLT}
         p2      {R_PLT} {B_PLT}
       endi
     endp
    endt
  enddiatom

$ --- TRACERS ---
  tracer points
    lagrangian Tracer 1  x  {C_MDL}        y {H_ROD}   $ Center of Rod Head
    lagrangian tracer 2  x  {C_MDL}        y {T_ROD}   $ Center of Rod Tail
    lagrangian tracer 3  x  {C_MDL}        y {F_PLT}   $ Center of Plate Front
    lagrangian tracer 4  x  {R_PLT-S_CEL}  y {F_PLT}   $ Edge of Plate Front
    lagrangian tracer 5  x  {R_ROD}        y {F_PLT}   $ Edge of Rod on Plate Front
  end

  plot, exotracer
    file = 'tracer.exo'
  end

$ plot, vtk mesh
$   file = 'hohlerstilprha'
$ end

end
```

```
$ === MATERIAL ===
material 1              $ 93% WHA
  model = 1
end
model 1 cth elastic plastic
  eos model      = 100
  yield model    = 10
$  fracture model = 1000
end
model 10 johnson cook ep
  ajo = 1.365e9         $ Hohler & Stilp
  bjo = 0.1765e9
  cjo = 0.016
  mjo = 1.00
  njo = 0.12
  tjo = 3695.
  poisson = 0.281
end
model 100, keos sesame
  feos = 'sesame'
  neos = 3550           $ TUNGSTEN
  sr   = 1.094          $ Scaled for 17.760 g/cc
  clip = 1.0
end

material 2              $ HzB Steel
  model = 2
end
model 2 cth elastic plastic
  eos model      = 200
  yield model    = 20
end
model 20 johnson cook ep
  ajo=0.810e9           $ Hohler & Stilp HzB
  bjo=0.5095e9
  cjo=0.014
  mjo=1.030
  njo=0.260
  tjo=1818.
  poisson = 0.299
end
model 200, keos sesame
  feos = 'sesame'
  neos = 2150           $ Iron
  sr   = 1.003          $ Scaled for 7.85 g/cc
  clip = 1.0
end

exit
```

## [hohlerstilprha.inp] for DNR_G_P15

```
$ {include("/home/bypark/common/units.txt")}
$ {_FORMAT="%.10g"}
$ --- COMMENTS ---
$     Author:          Brian Leavy
$     Modified:                Byoung Yoon Park 12-02-2011
$     Experiment:      Hohler & Stilp W rod vs RHA
$     Comments:                Validation test for X-FEM in ALEGRA

$=== VARIABLES====
$ {include("parameters.txt")}
$ Time Interval:    {T_INT = 1.0e-6} s
$ Plot Interval:    {P_INT = T_INT} s

$ === EXECUTION CONTROL ===
$ --- Initiation and Termination
Title
Hohler-Stilprha {T_CAS}, v={V_ROD} m/s, R={R_ROD*m_mm} mm, L={L_ROD*m_cm} cm, CELL={S_CEL*m_mm}
mm

units, si
READ RESTART DUMP = -1        $ Restart at the latest available restart dump
termination time, {tt=160.0e-6}       $ Simulation terminated at {tt*s_mus} mus.
TERMINATION CPU {tc=6.*h_s}   $ Run will be terminated within CPU time 1hr/64nodes(Agg)
$termination cycle, 1
CHECK SHUTDOWN FILE {csf=2}m          $ Check shutdown file every {csf} minutes
EMIT RESTART, TIME INTERVAL {T_INT} $ Make dmp file every {T_INT*s_mus} mus.
```

```
$--- I/O Control
emit plot, time interval={P_INT} $ s
emit hisplt, cycle interval=10

plot variables
  no underscores
  velocity
  density
  density,avg
  temperature
  temperature,avg
  pressure
  pressure,avg
  mat_min_coords
  mat_max_coords
end

history plot variables
  no underscores
  velocity
  density
  temperature
  pressure
end

spy

  PlotTime(0.0,{P_INT});

  define main()
  \{
    pprintf(" PLOT: Cycle=%d, Time=%e\n",CYCLE,TIME);
    % ListVariables();

    Image("HohlerStilpRha",WHITE,BLACK);
      Label("{T_CAS}, v={V_ROD} m/s, Graded cell={S_CEL*m_mm} mm");
      SMOOTH_SHADING = OFF;
      ColorMapRange(0.,20000.,LIN_MAP);
      % AutoScaleMap("DENSITY",0.,20000.);
      DrawColorMap("DENSITY",0.1,0.3,0.3,0.8);
      Plot2D("DENSITY");
      Color(PURPLE);
      Draw2DMatContour;

      Color(BLACK);
      DrawText(sprintf("t = %.2f ~m~s",1.e6*TIME),0.4,0.05);
      Color(BLACK);

      LogoShading(ON);
      LogoText(ON);
      LogoColors(BLACK,CYAN,BLACK);

      LogoPosition(0.0,0.0,0.4,0.15);
      DrawSNL_Logo(1.3);
    EndImage;
  \}
endspy

$ === PHYSICS INPUT===
solid dynamics
  cylindrical
  constant volume fraction algorithm
  end

  domain
    pattern reconstruction
    interface order 2 0 1
    pattern smoothing = off
    pattern fragment motion = off
  end

  time step scale, {tss=.4}  $ {tss} times of the value of the calculated stable time step.

$ --- MESH ---
$BX :{BX = 1} $ Number of Blocks in X
$BY :{BY = 1} $ Number of Blocks in Y
$NX_TOT :{NX_TOT = int((R_PLT/S_CEL)/BX)}
$NY_TOT :{NY_TOT = int((L_MDL/S_CEL)/BY)}
$NX :{NX = NX_TOT/BX}
$NY :{NY = NY_TOT/BY}
```

```
$NSLOTS :{NSLOTS = BX*BY}
$NUM_CELLS :{NUM_CELLS = NX_TOT*NY_TOT}
$R_DER :{R_DER = 4.*R_ROD} $ Dense element radius bound (R-dir)
$Z_DEU :{Z_DEU = 0.078}    $ Dense element upper bound (Z-dir) (hole depth is 0.0741 at 3000 m/s)
$Z_DEL :{Z_DEL = 0.000}    $ Dense element lower bound (Z-dir)
$F_DER :{F_DER = 0.1}      $ Increase Rate (R-dir), The larger, the smaller interval
$F_DER :{F_DEU = 0.7}      $ Increase Factor (+Z-dir), The larger, the smaller interval
$F_DEL :{F_DEL = 0.3}      $ Increase Factor (-Z-dir), The larger, the larger interval
mesh, inline
  rectilinear
    bx = {BX}
    by = {BY}
    nx = {NX}
    ny = {NY}
    gmin = {C_MDL} {F_MDL}
    gmax = {NX_TOT*BX*S_CEL}  {F_MDL+NY_TOT*BY*S_CEL}
  end
  set assign
    sideset,ilo,30
    sideset,ihi,10
    sideset,jlo,40
    sideset,jhi,20
  end
  USER DEFINED ELEMENT DENSITY, X
    "
      field=1;
      if(coord <  {R_DER}) {"{"}field = 1;{"}"}
      if(coord >= {R_DER}) {"{"}field = 1.*exp(-100.*((coord)-{R_DER*F_DER}));{"}"}
    "
  END
  USER DEFINED ELEMENT DENSITY, Y
    "
      field=1;
      if(coord <  {Z_DEU}) {"{"}field = 1;{"}"}
      if(coord >= {Z_DEU}) {"{"}field = 1.*exp(-80.*((coord)-{Z_DEU*F_DEU}));{"}"}
      if(coord <= {Z_DEL}) {"{"}field = 1.*exp( 70.*((coord)-{Z_DEU*F_DEL}));{"}"}
      if(coord <  {T_ROD}) {"{"}field = 1;{"}"}
    "
  END
end
$$
$ --- BOUNDARY CONDITION ---
  no displacement, sideset 20,z $ +Z
  no displacement, sideset 10,r $ +R
  no displacement, sideset 30,r $ -R = 0

  block 1
    eulerian mesh
    add diatom input
    user defined advection
      mixed cells, donor advection
      mixed neighbors, donor advection
      mixed stencil, donor advection
      element, donor advection
    end
  end

$ --- MATERIAL INSERTION ---
$-----------------------------------------
$  material 1, rod, 93% WHA, Tungsten
$  material 2, plate, HzB Steel
$-----------------------------------------
  diatom
    translate(0.,{H_ROD})
     package 'ROD'
       material 1
       yvelocity {V_ROD}
       insert box
         p1      {C_MDL} {H_ROD}
         p2      {R_ROD} {T_ROD}
       endi
     endp
    endt
    translate(0.,{F_PLT})
     package 'PLATE'
       material 2
       insert box
         p1      {C_MDL} {F_PLT}
         p2      {R_PLT} {B_PLT}
       endi
     endp
```

```
    endt
  enddiatom

$ --- TRACERS ---
  tracer points
    lagrangian Tracer 1  x  {C_MDL}        y {H_ROD}   $ Center of Rod Head -- Tracer H
    lagrangian tracer 2  x  {C_MDL}        y {T_ROD}   $ Center of Rod Tail
    lagrangian tracer 3  x  {C_MDL}        y {F_PLT}   $ Center of Plate Front
    lagrangian tracer 4  x  {R_PLT-S_CEL}  y {F_PLT}  $ Edge of Plate Front -- Tracer P
    lagrangian tracer 5  x  {R_ROD}        y {F_PLT}   $ Edge of Rod on Plate Front
  end

  plot, exotracer
    file = 'tracer.exo'
  end

$ plot, vtk mesh
$   file = 'hohlerstilprha'
$ end

end

$ === MATERIAL ===
material 1              $ 93% WHA
  model = 1
end
model 1 cth elastic plastic
  eos model      = 100
  yield model    = 10
$  fracture model = 1000
end
model 10 johnson cook ep
  ajo = 1.365e9         $ Hohler & Stilp
  bjo = 0.1765e9
  cjo = 0.016
  mjo = 1.00
  njo = 0.12
  tjo = 3695.
  poisson = 0.281
end
model 100, keos sesame
  feos = 'sesame'
  neos = 3550            $ TUNGSTEN
  sr   = 1.094           $ Scaled for 17.760 g/cc
  clip = 1.0
end

material 2               $ HzB Steel
  model = 2
end
model 2 cth elastic plastic
  eos model      = 200
  yield model    = 20
end
model 20 johnson cook ep
  ajo=0.810e9            $ Hohler & Stilp HzB
  bjo=0.5095e9
  cjo=0.014
  mjo=1.030
  njo=0.260
  tjo=1818.
  poisson = 0.299
end
model 200, keos sesame
  feos = 'sesame'
  neos = 2150            $ Iron
  sr   = 1.003           $ Scaled for 7.85 g/cc
  clip = 1.0
end

exit
```

## Appendix 2: Input deck for 4x18fixed

[parameters.txt]

```
$
$ Define Parameters
$
$ Test Case:                    T_CAS = {T_CAS='4x18fx0500'}
$ Cell size:                    S_CEL = {S_CEL=0.17*mm_m} m
$ Model Center (X):             C_MDL = {C_MDL=  0.00} m
$ Radius of Plate (X):          R_PLT = {R_PLT= 40.0*mm_m} m
$ Thickness of Plate (Y):       T_PLT = {T_PLT= 180.0*mm_m} m
$ Radius of Rod (X):            R_ROD = {R_ROD= 2.5*mm_m} m
$ Lengh of Rod (Y):             L_ROD = {L_ROD= 50.0*mm_m} m
$ Velocity of Rod:              V_ROD = {V_ROD= 500} m/s
$ Front of Plate (Y):           F_PLT = {F_PLT= 0.00} m
$ Back of Plate (Y):            B_PLT = {B_PLT= F_PLT+T_PLT} m
$ Head of Rod (Y):              H_ROD = {H_ROD= F_PLT} m
$ Tail of Rod (Y):              T_ROD = {T_ROD= H_ROD-L_ROD} m
$ Back of Model (Y):            B_MDL = {B_MDL= R_PLT} m
$ Front of 1st Graded Area (Y): F_1GA = {F_1GA= 78.*mm_m} m (hole depth is 0.0741 at 3000 m/s)
$ Radius of 1st Graded Area (X): R_1GA = {R_1GA= 4.*R_ROD} m
$ Gap between Rod tail and Fornt of Model (Y): L_GAP = {L_GAP= S_CEL} m
$ Front of Model (Y):           F_MDL = {F_MDL= T_ROD-L_GAP} m
$ Length of Model (Y):          L_MDL = {L_MDL= T_PLT+L_ROD+L_GAP} m
```

Note: V_ROD varied from 500 m/s to 3000 m/s for the projectile rod velocities.

[hohlerstilprha.inp]

```
$ {include("/home/bypark/common/units.txt")}
$ {_FORMAT="%.10g"}
$ --- COMMENTS ---
$     Author:          Brian Leavy
$     Modified:               Byoung Yoon Park 12-02-2011
$     Experiment:      Hohler & Stilp W rod vs RHA
$     Comments:                Validation test for X-FEM in ALEGRA

$=== VARIABLES====
$ {include("parameters.txt")}
$ Time Interval:    {T_INT = 1.0e-6} s
$ Plot Interval:    {P_INT = T_INT} s

$ === EXECUTION CONTROL ===
$ --- Initiation and Termination
Title
Hohler-Stilprha {T_CAS}, v={V_ROD} m/s, Plate Thick={T_PLT*m_cm} cm, CELL={S_CEL*m_mm} mm

units, si
READ RESTART DUMP = -1        $ Restart at the latest available restart dump
termination time, {tt=160.0e-6}       $ Simulation terminated at {tt*s_mus} mus.
TERMINATION CPU {tc=9.*h_s}   $ Run will be terminated within CPU time {tc*s_h} hr/64nodes(XFEM)
$termination cycle, 1
CHECK SHUTDOWN FILE {csf=2}m         $ Check shutdown file every {csf} minutes
EMIT RESTART, TIME INTERVAL {T_INT} $ Make dmp file every {T_INT*s_mus} mus.

$--- I/O Control
emit plot, time interval={P_INT} $ s
$emit plot, cycle interval=10 from time 7.e-5 to 15.e-5
emit hisplt, cycle interval=10
$emit hisplt, time interval={T_INT} $ s
$emit hisplt, cycle interval=1 from time 7.e-5 to 15.e-5

plot variables
  no underscores
  velocity
  density
  density,avg
  temperature
  temperature,avg
  pressure
  pressure,avg
  mat_min_coords
  mat_max_coords
end

history plot variables
  no underscores
  velocity
```

```
  density
  temperature
  pressure
end

spy

  PlotTime(0.0,{P_INT});

  define main()
  \{
    pprintf(" PLOT: Cycle=%d, Time=%e\n",CYCLE,TIME);
    % ListVariables();

    Image("HohlerStilpRha",WHITE,BLACK);
      Label("{T_CAS}, v={V_ROD} m/s, Plate Thick={T_PLT*m_cm} cm");
      SMOOTH_SHADING = OFF;
      ColorMapRange(0.,20000.,LIN_MAP);
      % AutoScaleMap("DENSITY",0.,20000.);
      DrawColorMap("DENSITY",0.1,0.3,0.3,0.8);
      Plot2D("DENSITY");
      Color(PURPLE);
      Draw2DMatContour;

      Color(BLACK);
      DrawText(sprintf("t = %.2f ~m~s",1.e6*TIME),0.4,0.05);
      Color(BLACK);

      LogoShading(ON);
      LogoText(ON);
      LogoColors(BLACK,CYAN,BLACK);

      LogoPosition(0.0,0.0,0.4,0.15);
      DrawSNL_Logo(1.3);
    EndImage;
  \}
endspy

$ === PHYSICS INPUT===
solid dynamics
  cylindrical
  constant volume fraction algorithm
  end

  xfem
    tangential search tolerance, 0.05
    maxenf iterations, 100
    gap rate tolerance, 1.e-8
    mspair 2,1
  end

  domain
    remap method, intersection
    pattern reconstruction
    interface order 2 0 1
    pattern smoothing = off
    pattern fragment motion = off
  end

  time step scale, {tss=.4}  $ {tss} times of the value of the calculated stable time step.

$ --- MESH ---
$BX :{BX = 1} $ Number of Blocks in X
$BY :{BY = 1} $ Number of Blocks in Y
$NX_TOT :{NX_TOT = int((R_PLT/S_CEL)/BX)}
$NY_TOT :{NY_TOT = int((L_MDL/S_CEL)/BY)}
$NX :{NX = NX_TOT/BX}
$NY :{NY = NY_TOT/BY}
$NSLOTS :{NSLOTS = BX*BY}
$NUM_CELLS :{NUM_CELLS = NX_TOT*NY_TOT}
$R_DER :{R_DER = 4.*R_ROD} $ Dense element radius bound (R-dir)
$Z_DEU :{Z_DEU = 0.078}    $ Dense element upper bound (Z-dir) (hole depth is 0.0741 at 3000 m/s)
$Z_DEL :{Z_DEL = 0.000}    $ Dense element lower bound (Z-dir)
$I_DER :{I_DER = -100.}    $ Increase Rate (R-dir), The larger, the larger increase rate
$I_DEU :{I_DEU = -40.0}    $ Increase Rate (+Z-dir), The larger, the larger increase rate
$I_DEL :{I_DEL =  70.0}    $ Increase Rate (-Z-dir), The larger, the smaller increase rate
$F_DER :{F_DER = 0.1}      $ Increase Factor (R-dir), The larger, the smaller interval at end
$F_DEU :{F_DEU = 0.9}      $ Increase Factor (+Z-dir), The larger, the smaller interval at end
$F_DEL :{F_DEL = 0.2}      $ Increase Factor (-Z-dir), The larger, the larger interval at end
$$$ T_PLT=160 mm, I_DEU=-50, S_CEL=0.15
$$$ T_PLT=170 mm, I_DEU=-45, S_CEL=0.2
```

```
$$$ T_PLT=180 mm, I_DEU=-40, S_CEL=0.17

mesh, inline
  rectilinear
    bx = {BX}
    by = {BY}
    nx = {NX}
    ny = {NY}
    gmin = {C_MDL} {F_MDL}
    gmax = {NX_TOT*BX*S_CEL}  {F_MDL+NY_TOT*BY*S_CEL}
  end
  set assign
    sideset,ilo,30
    sideset,ihi,10
    sideset,jlo,40
    sideset,jhi,20
  end
  USER DEFINED ELEMENT DENSITY, X
    "
      field=1;
      if(coord <  {R_DER}) {"{"}field = 1;{"}"}
      if(coord >= {R_DER}) {"{"}field = 1.*exp({I_DER}*((coord)-{R_DER*F_DER}));{"}"}
    "
  END
  USER DEFINED ELEMENT DENSITY, Y
    "
      field=1;
      if(coord <  {Z_DEU}) {"{"}field = 1;{"}"}
      if(coord >= {Z_DEU}) {"{"}field = 1.*exp({I_DEU}*((coord)-{Z_DEU*F_DEU}));{"}"}
      if(coord <= {Z_DEL}) {"{"}field = 1.*exp({I_DEL}*((coord)-{Z_DEU*F_DEL}));{"}"}
      if(coord <  {T_ROD}) {"{"}field = 1;{"}"}
    "
  END
end
$$
$ --- BOUNDARY CONDITION ---
  no displacement, sideset 20,z $ +Z
  no displacement, sideset 10,r $ +R
  no displacement, sideset 30,r $ -R = 0

  block 1
    EULERIAN MESH
    add diatom input
  end

$ --- MATERIAL INSERTION ---
$----------------------------------------
$  material 1, rod, 93% WHA, Tungsten
$  material 2, plate, HzB Steel
$----------------------------------------
  diatom
    translate(0.,{H_ROD})
     package 'ROD'
       material 1
       yvelocity {V_ROD}
       insert box
         p1      {C_MDL} {H_ROD}
         p2      {R_ROD} {T_ROD}
       endi
     endp
    endt
    translate(0.,{F_PLT})
     package 'PLATE'
       material 2
       insert box
         p1      {C_MDL} {F_PLT}
         p2      {R_PLT} {B_PLT}
       endi
     endp
    endt
  enddiatom

$ --- TRACERS ---
  tracer points
    lagrangian Tracer 1  x  {C_MDL}        y {H_ROD}   $ Center of Rod Head   -- Tracer H
    lagrangian tracer 2  x  {C_MDL}        y {T_ROD}   $ Center of Rod Tail
    lagrangian tracer 3  x  {C_MDL}        y {F_PLT}   $ Center of Plate Front
    lagrangian tracer 4  x  {R_PLT-S_CEL}  y {F_PLT}   $ Edge of Plate Front  -- Tracer P
    lagrangian tracer 5  x  {R_ROD}        y {F_PLT}   $ Edge of Rod on Plate Front
  end
```

```
  plot, exotracer
    file = 'tracer.exo'
  end

$ plot, vtk mesh
$   file = 'hohlerstilprha'
$ end

end

$ === MATERIAL ===
material 1              $ 93% WHA
  model = 1
end
model 1 cth elastic plastic
  eos model      = 100
  yield model    = 10
$  fracture model = 1000
end
model 10 johnson cook ep
  ajo = 1.365e9         $ Hohler & Stilp
  bjo = 0.1765e9
  cjo = 0.016
  mjo = 1.00
  njo = 0.12
  tjo = 3695.
  poisson = 0.281
end
model 100, keos sesame
  feos = 'sesame'
  neos = 3550            $ TUNGSTEN
  sr   = 1.094           $ Scaled for 17.760 g/cc
  clip = 1.0
end

material 2               $ HzB Steel
  model = 2
end
model 2 cth elastic plastic
  eos model      = 200
  yield model    = 20
end
model 20 johnson cook ep
  ajo=0.810e9            $ Hohler & Stilp HzB
  bjo=0.5095e9
  cjo=0.014
  mjo=1.030
  njo=0.260
  tjo=1818.
  poisson = 0.299
end
model 200, keos sesame
  feos = 'sesame'
  neos = 2150            $ Iron
  sr   = 1.003           $ Scaled for 7.85 g/cc
  clip = 1.0
end

exit
```

## Appendix 3: Input deck for 5x12fixed

[parameters.txt]

```
$
$ Define Parameters
$
$ Test Case:                    T_CAS = {T_CAS='5x12fx0500'}
$ Cell size:                    S_CEL = {S_CEL=0.17*mm_m} m
$ Model Center (X):             C_MDL = {C_MDL=  0.00} m
$ Radius of Plate (X):          R_PLT = {R_PLT= 50.0*mm_m} m
$ Thickness of Plate (Y):       T_PLT = {T_PLT= 120.0*mm_m} m
$ Radius of Rod (X):            R_ROD = {R_ROD= 2.5*mm_m} m
$ Lengh of Rod (Y):             L_ROD = {L_ROD= 50.0*mm_m} m
$ Velocity of Rod:              V_ROD = {V_ROD= 500} m/s
$ Front of Plate (Y):           F_PLT = {F_PLT= 0.00} m
$ Back of Plate (Y):            B_PLT = {B_PLT= F_PLT+T_PLT} m
$ Head of Rod (Y):              H_ROD = {H_ROD= F_PLT} m
$ Tail of Rod (Y):              T_ROD = {T_ROD= H_ROD-L_ROD} m
$ Back of Model (Y):            B_MDL = {B_MDL= R_PLT} m
$ Front of 1st Graded Area (Y): F_1GA = {F_1GA= 78.*mm_m} m (hole depth is 0.0741 at 3000 m/s)
$ Radius of 1st Graded Area (X): R_1GA = {R_1GA= 4.*R_ROD} m
$ Gap between Rod tail and Fornt of Model (Y): L_GAP = {L_GAP= S_CEL} m
$ Front of Model (Y):           F_MDL = {F_MDL= T_ROD-L_GAP} m
$ Length of Model (Y):          L_MDL = {L_MDL= T_PLT+L_ROD+L_GAP} m
```

Note: V_ROD varied from 500 m/s to 3000 m/s for the projectile rod velocities.

[hohlerstilprha.inp]

```
$ {include("/home/bypark/common/units.txt")}
$ {_FORMAT="%.10g"}
$ --- COMMENTS ---
$     Author:          Brian Leavy
$     Modified:                Byoung Yoon Park 12-02-2011
$     Experiment:      Hohler & Stilp W rod vs RHA
$     Comments:                Validation test for X-FEM in ALEGRA

$=== VARIABLES====
$ {include("parameters.txt")}
$ Time Interval:    {T_INT = 1.0e-6} s
$ Plot Interval:    {P_INT = T_INT} s

$ === EXECUTION CONTROL ===
$ --- Initiation and Termination
Title
Hohler-Stilprha {T_CAS}, v={V_ROD} m/s, Plate Thick={T_PLT*m_cm} cm, CELL={S_CEL*m_mm} mm

units, si
READ RESTART DUMP = -1        $ Restart at the latest available restart dump
termination time, {tt=160.0e-6}       $ Simulation terminated at {tt*s_mus} mus.
TERMINATION CPU {tc=5.*h_s}   $ Run will be terminated within CPU time {tc*s_h} hr/64nodes(XFEM)
$termination cycle, 1
CHECK SHUTDOWN FILE {csf=2}m          $ Check shutdown file every {csf} minutes
EMIT RESTART, TIME INTERVAL {T_INT} $ Make dmp file every {T_INT*s_mus} mus.

$--- I/O Control
emit plot, time interval={P_INT} $ s
$emit plot, cycle interval=10 from time 7.e-5 to 15.e-5
emit hisplt, cycle interval=10
$emit hisplt, time interval={T_INT} $ s
$emit hisplt, cycle interval=1 from time 7.e-5 to 15.e-5

plot variables
  no_underscores
  velocity
  density
  density,avg
  temperature
  temperature,avg
  pressure
  pressure,avg
  mat_min_coords
  mat_max_coords
end

history plot variables
  no_underscores
  velocity
  density
  temperature
```

```
  pressure
end

spy

  PlotTime(0.0,{P_INT});

  define main()
  \{
    pprintf(" PLOT: Cycle=%d, Time=%e\n",CYCLE,TIME);
    % ListVariables();

    Image("HohlerStilpRha",WHITE,BLACK);
      Label("{T_CAS}, v={V_ROD} m/s, Plate Thick={T_PLT*m_cm} cm");
      SMOOTH_SHADING = OFF;
      ColorMapRange(0.,20000.,LIN_MAP);
      % AutoScaleMap("DENSITY",0.,20000.);
      DrawColorMap("DENSITY",0.1,0.3,0.3,0.8);
      Plot2D("DENSITY");
      Color(PURPLE);
      Draw2DMatContour;

      Color(BLACK);
      DrawText(sprintf("t = %.2f ~m~s",1.e6*TIME),0.4,0.05);
      Color(BLACK);

      LogoShading(ON);
      LogoText(ON);
      LogoColors(BLACK,CYAN,BLACK);

      LogoPosition(0.0,0.0,0.4,0.15);
      DrawSNL_Logo(1.3);
    EndImage;
  \}
endspy

$ === PHYSICS INPUT===
solid dynamics
  cylindrical
  constant volume fraction algorithm
  end

  xfem
    tangential search tolerance, 0.05
    maxenf iterations, 100
    gap rate tolerance, 1.e-8
    mspair 2,1
  end

  domain
    remap method, intersection
    pattern reconstruction
    interface order 2 0 1
    pattern smoothing = off
    pattern fragment motion = off
  end

  time step scale, {tss=.4}  $ {tss} times of the value of the calculated stable time step.

$ --- MESH ---
$BX :{BX = 1} $ Number of Blocks in X
$BY :{BY = 1} $ Number of Blocks in Y
$NX_TOT :{NX_TOT = int((R_PLT/S_CEL)/BX)}
$NY_TOT :{NY_TOT = int((L_MDL/S_CEL)/BY)}
$NX :{NX = NX_TOT/BX}
$NY :{NY = NY_TOT/BY}
$NSLOTS :{NSLOTS = BX*BY}
$NUM_CELLS :{NUM_CELLS = NX_TOT*NY_TOT}
$R_DER :{R_DER = 4.*R_ROD} $ Dense element radius bound (R-dir)
$Z_DEU :{Z_DEU = 0.078}    $ Dense element upper bound (Z-dir) (hole depth is 0.0741 at 3000 m/s)
$Z_DEL :{Z_DEL = 0.000}    $ Dense element lower bound (Z-dir)
$I_DER :{I_DER = -100.}    $ Increase Rate (R-dir), The larger, the larger increase rate
$I_DEU :{I_DEU = -80.0}    $ Increase Rate (+Z-dir), The larger, the larger increase rate
$I_DEL :{I_DEL =  70.0}    $ Increase Rate (-Z-dir), The larger, the smaller increase rate
$F_DER :{F_DER = 0.1}      $ Increase Factor (R-dir), The larger, the smaller interval at end
$F_DEU :{F_DEU = 0.7}      $ Increase Factor (+Z-dir), The larger, the smaller interval at end
$F_DEL :{F_DEL = 0.3}      $ Increase Factor (-Z-dir), The larger, the larger interval at end
$$$ T_PLT=160 mm, R_PLT= 40, I_DEU=-50, S_CEL=0.15
$$$ T_PLT=170 mm, R_PLT= 40, I_DEU=-45, S_CEL=0.2
$$$ T_PLT=180 mm, R_PLT= 40, I_DEU=-40, S_CEL=0.17
$$$ T_PLT=120 mm, R_PLT= 50, I_DEU=-80, S_CEL=0.17
```

```
mesh, inline
  rectilinear
    bx = {BX}
    by = {BY}
    nx = {NX}
    ny = {NY}
    gmin = {C_MDL} {F_MDL}
    gmax = {NX_TOT*BX*S_CEL}  {F_MDL+NY_TOT*BY*S_CEL}
  end
  set assign
    sideset,ilo,30
    sideset,ihi,10
    sideset,jlo,40
    sideset,jhi,20
  end
  USER DEFINED ELEMENT DENSITY, X
    "
      field=1;
      if(coord <  {R_DER}) {"{"}field = 1;{"}"}
      if(coord >= {R_DER}) {"{"}field = 1.*exp({I_DER}*((coord)-{R_DER*F_DER}));{"}"}
    "
  END
  USER DEFINED ELEMENT DENSITY, Y
    "
      field=1;
      if(coord <  {Z_DEU}) {"{"}field = 1;{"}"}
      if(coord >= {Z_DEU}) {"{"}field = 1.*exp({I_DEU}*((coord)-{Z_DEU*F_DEU}));{"}"}
      if(coord <= {Z_DEL}) {"{"}field = 1.*exp({I_DEL}*((coord)-{Z_DEU*F_DEL}));{"}"}
      if(coord <  {T_ROD}) {"{"}field = 1;{"}"}
    "
  END
end
$$
$ --- BOUNDARY CONDITION ---
  no displacement, sideset 20,z $ +Z
  no displacement, sideset 10,r $ +R
  no displacement, sideset 30,r $ -R = 0

  block 1
    EULERIAN MESH
    add diatom input
  end

$ --- MATERIAL INSERTION ---
$----------------------------------------
$  material 1, rod, 93% WHA, Tungsten
$  material 2, plate, HzB Steel
$----------------------------------------
  diatom
    translate(0.,{H_ROD})
     package 'ROD'
       material 1
       yvelocity {V_ROD}
       insert box
         p1      {C_MDL} {H_ROD}
         p2      {R_ROD} {T_ROD}
       endi
     endp
    endt
    translate(0.,{F_PLT})
     package 'PLATE'
       material 2
       insert box
         p1      {C_MDL} {F_PLT}
         p2      {R_PLT} {B_PLT}
       endi
     endp
    endt
  enddiatom

$ --- TRACERS ---
  tracer points
    lagrangian Tracer 1  x  {C_MDL}        y {H_ROD}   $ Center of Rod Head   -- Tracer H
    lagrangian tracer 2  x  {C_MDL}        y {T_ROD}   $ Center of Rod Tail
    lagrangian tracer 3  x  {C_MDL}        y {F_PLT}   $ Center of Plate Front
    lagrangian tracer 4  x  {R_PLT-S_CEL}  y {F_PLT}   $ Edge of Plate Front  -- Tracer P
    lagrangian tracer 5  x  {R_ROD}        y {F_PLT}   $ Edge of Rod on Plate Front
  end

  plot, exotracer
```

```
    file = 'tracer.exo'
  end

$ plot, vtk mesh
$   file = 'hohlerstilprha'
$ end

end

$ === MATERIAL ===
material 1              $ 93% WHA
  model = 1
end
model 1 cth elastic plastic
  eos model      = 100
  yield model    = 10
$  fracture model = 1000
end
model 10 johnson cook ep
  ajo = 1.365e9         $ Hohler & Stilp
  bjo = 0.1765e9
  cjo = 0.016
  mjo = 1.00
  njo = 0.12
  tjo = 3695.
  poisson = 0.281
end
model 100, keos sesame
  feos = 'sesame'
  neos = 3550            $ TUNGSTEN
  sr   = 1.094           $ Scaled for 17.760 g/cc
  clip = 1.0
end

material 2               $ HzB Steel
  model = 2
end
model 2 cth elastic plastic
  eos model      = 200
  yield model    = 20
end
model 20 johnson cook ep
  ajo=0.810e9            $ Hohler & Stilp HzB
  bjo=0.5095e9
  cjo=0.014
  mjo=1.030
  njo=0.260
  tjo=1818.
  poisson = 0.299
end
model 200, keos sesame
  feos = 'sesame'
  neos = 2150            $ Iron
  sr   = 1.003           $ Scaled for 7.85 g/cc
  clip = 1.0
end

exit
```

# DISTRIBUTION

## External Distribution

1 R. B. Leavy
U.S. Army Research Laboratory
ATTN: RDRL-WMP-C
Aberdeen Proving Grounds, MD 21005

1 R. L. Doney
U.S. Army Research Laboratory
ATTN: RDRL-WMP-D
Aberdeen Proving Grounds, MD 21005

1 A. J. Porwitzky
U.S. Army Research Laboratory
ATTN: RDRL-WMP-A
Aberdeen Proving Grounds, MD 21005

1 J. R. Houskamp
U.S. Army Research Laboratory
ATTN: RDRL-WMP-D
Aberdeen Proving Grounds, MD 21005

## Sandia Internal Distribution

| | | | |
|---|---|---|---|
| 1 | MS 0380 | 1443 | G. T. Sharp |
| 1 | MS 0735 | 6910 | J. A. Merson |
| 5 | MS 0751 | 6914 | B. Y. Park |
| 1 | MS 0751 | 6914 | M. Y. Lee |
| 1 | MS 1318 | 1440 | T. G. Trucano |
| 1 | MS 1323 | 1443 | J. H. J. Niederhaus |
| 1 | MS 1323 | 1443 | T. E. Voth |
| 1 | MS 1323 | 1443 | S. J. Mosso |
| 1 | MS 1323 | 1443 | R. M. J. Kramer |
| 1 | MS 1323 | 1443 | W. J. Rider |
| 1 | MS 1323 | 1443 | A. C. Robinson |
| 1 | MS 1323 | 1443 | O. E. Strack |
| 1 | MS 1454 | 2556 | T. Pfeifle |
| 1 | MS 0899 | 9536 | Technical Library |

Sandia National Laboratories